Kinetic model development and CFD simulation of a silicon oxynitride (SiO_xN_y) CVD process from TDMSA/O_2 mixtures

Tryfon TSIROS

Supervisors:

Andreas G. BOUDOUVIS (NTUA)
Hugues VERGNES, Brigitte CAUSSAT, Constantin VAHLAS (ENSIACET)

25/09/2020

Abstract

Silicon oxynitrides thin films have a very wide application in optical devices, dielectric materials, and optical waveguide materials. Additionally, SiO_xN_y films also have high chemical stability, high resistance to impurity diffusion, and water vapor permeability, properties that are highly required for applications in barrier devices such as gas barriers, making this material a promising candidate. The present thesis focuses on the formation of thin SiO_xN_y films through a relatively moderate temperature thermal CVD process (T=650°C) at atmospheric pressure. The chemistry selected to undertake this task is a mixture of tris-dimethylsilyl-amine (TDMSA) and O_2, a novel chemistry where nitrogen and silicon atoms originate from the precursor itself and nitrogen not being supplied by an external gas source like ammonia. For this research, a tubular horizontal hot-wall reactor configuration has been utilized to produce the silicon oxynitride material and the development of the respective chemical model. Ellipsometry and FTIR are the main instruments used for the solid phase analysis and characterization of the films, with Ellipsometry supplying a large amount of data relating to the deposition rate and composition, aiding the simulations substantially. The development of the model is additionally also based on gas phase results from GC-MS, liquid NMR and ESR analyses. The combined use of solid-state and gas phase results were thus used as the main feedback for the present work, in order to develop an apparent kinetic model, that could replicate the deposition mechanism from the TDMSA+O_2 chemical system in a simplified manner. Lastly, the kinetic model constructed for this system is implemented in the simulation software ANSYS® FLUENT® 18.2 and aims to recreate the experiments with satisfactory accuracy through the use of computational fluid dynamics, opening the way to further possibilities for process optimization.

Key words: Computational Fluid Dynamics, CVD, Silicon oxynitrides, Simulation, Kinetic Model, Gas phase analysis.

Περίληψη

Τα οξινιτρίδια του πυριτίου έχουν ευρεία εφαρμογή στη βιομηχανία. Χρησιμοποιούνται σε οπτικές συσκευές, διηλεκτρικά υλικά και υλικά οπτικών κυματοδηγών. Οι μεμβράνες SiO_xN_y έχουν επίσης υψηλή χημική σταθερότητα καθώς και υψηλή αντοχή στη διάχυση και διαπερατότητα υδρατμών. Η συγκεκριμένη έρευνα εξετάζει τη δημιουργία λεπτών μεμβρανών SiO_xN_y διαμέσω μιας διεργασίας χημικής απόθεσης ατμών (CVD) χαμηλής θερμοκρασίας (T = 650 ° C). Η χημεία που επιλέχθηκε για να αναλάβει αυτό το έργο είναι ένα μείγμα τρις-διμεθυλσιλυλ-αμίνης (TDMSA) και O_2, μιας πρωτοποριακής χημείας όπου το άζωτο και το πυρίτιο προέρχονται από την ίδια πρόδρομη ένωση. Για αυτόν τον σκοπό, κατασκευάστηκε κατάλληλος αντιδραστήρας και επιλέχθηκαν κατάλληλες μέθοδοι ανάλυσης στερεής και αέριας φάσης έτσι ώστε να εξαχθούν οι απαραίτητες πληροφορίες για τη διαμόρφωση ενός κινητικού μοντέλου το οποίο θα εισαχθεί σε λογισμικό προσομοιώσεων με σκοπό τη βελτιστοποίηση της διεργασίας. Η συγκεκριμένη διπλωματική εργασία εστιάζει στην ανάπτυξη του κινητικού μοντέλου του αναφερόμενου χημικού συστήματος καθώς και στην πραγματοποίηση των προσομοιώσεων.

Η πρακτική εργασία πάνω στην οποία βασίζεται η παρούσα διπλωματική εργασία πραγματοποιήθηκε υπό το πλαίσιο του ERASMUS+ και συγκεκριμένα ανάμεσα στο Εθνικό Μετσόβιο Πολυτεχνείο (ΕΜΠ) και το Institut National Polytechnique της Τουλούζης (INPT). Συγκεκριμένα στο ινστιτούτο École Nationale Supérieure des Ingénieurs en Arts Chimiques et Technologiques (ENSIACET) ως μέρος του προγράμματος HEALTHYGLASS. Το εργαστήριο υπεύθυνο για την πρακτική ήταν το Laboratoire de Génie Chimique (LGC). Βέβαια, για την πραγματοποίηση της συγκεκριμένης έρευνας ήταν απαραίτητη η συμμετοχή αρκετών εργαστηρίων από όλη τη Γαλλία.

Η έρευνα ξεκίνησε με την επιλογή χημείας η οποία θα μπορούσε να εναποθέσει SiO_xN_y. Η τρις-διμεθυλσιλυλ-αμίνη (TDMSA), επιλέχθηκε για αυτόν τον σκοπό καθώς ανήκει στην οικογένεια των σιλυλαμίνων που είναι γενικά γνωστό ότι μπορούν να παράγουν Si_3N_4 κάτω από διεργασίες χημικής απόθεσης ατμών. Για την απόθεση αρχικά χρησιμοποιήθηκε μίγμα TDMSA + $O_2 + NH_3$ αλλά κατά τη διάρκεια των πειραμάτων έγινε αντιληπτό ότι η αμμωνία όχι μόνο δε συνεισφέρει στην απόθεση, άλλα δρα ως τροχοπέδη σε αυτήν. Γι' αυτόν το λόγο, το τελικό μίγμα που χρησιμοποιήθηκε για τη διαμόρφωση του κινητικού μοντέλου ήταν το TDMSA + O_2.

Σε αυτό το σημείο πρέπει να αναφέρουμε ότι το κινητικό μοντέλο που ερευνάται, το οποίο θα χρησιμοποιηθεί και για τις προσομοιώσεις αποτελεί ένα «φαινομενικό» κινητικό μοντέλο. Με τον όρο φαινομενικό χαρακτηρίζεται ένα μοντέλο το οποίο δεν αντιπροσωπεύει αυτό που πραγματικά συμβαίνει στο χημικό σύστημα, αλλά είναι ένα τεχνητό κινητικό μοντέλο το οποίο μπορεί να αναπαραγάγει τα πειραματικά αποτελέσματα στο περιβάλλον της προσομοίωσης αλλά παράλληλα είναι έντονα συνδεδεμένο με την πραγματικότητα μέσω των αποτελεσμάτων ανάλυσης στερεής και αέριας φάσης καθώς και μέσω βιβλιογραφικής έρευνας.

Τα πειράματα πραγματοποιήθηκαν σε έναν ειδικά διαμορφωμένο σωληνοειδή αντιδραστήρα μέσα στον οποίο τοποθετούνται κάθετα 18 υποστρώματα πυριτίου σε δειγματολήπτη.
Οι αρχικές συνθήκες όλων των πειραμάτων μπορούν να συνοψιστούν στον παρακάτω πίνακα.

Experiment Code	T (°C)	TDMSA $flow\ rate$ (sccm)	$O_2\ flow\ rate$ (sccm)	$NH_3\ flow\ rate$ (sccm)
TD3	650	6	0.6	40
TD4	650	2	2	20
TD5	650	2	0	20
TD6	650	2	0.6	20
TD7	650	2	0.6	0
TD8	650	2	0.6	40
TD9	650	2	0	0
TD11	650	2	0.3	0
TD12	650	2	0.6	0
TD14	625	2	1.2	0

Αν και αρχικά η αμμωνία συμμετείχε στα πειράματα αργότερα απορρίφθηκε ως αντιδρών καθιστώντας τα πειράματα που την συμπεριλαμβάνουν δευτερεύουσας σημασίας.

Η ανάλυση της στερεής φάσης των παραπάνω πειραμάτων πραγματοποιήθηκε μέσω της ελλειψομετρίας και του οργάνου FTIR, με την ελλειψομετρία να μας δίνει πληροφορίες σχετικά με το πάχος του εναποτιθέμενου υλικού καθώς και το ατομικό του ποσοστό σε άζωτο ενώ το FTIR σχετικά με τους δεσμούς που υπάρχουν στη δομή του επιστρώματος. Σε αυτό το σημείο έπρεπε να γίνει μια σημαντική παραδοχή, ότι το υλικό που παράγεται αποτελεί το άθροισμα δύο φάσεων.

$$SiO_2 + Si_3N_4 \rightarrow SiO_xN_y$$

Αυτή η παραδοχή ήταν απαραίτητη καθώς η ανάλυση της ελλειψομετρίας αδυνατούσε αρχικά να δώσει αξιόπιστα αποτελέσματα τα οποία να συμπεριλαμβάνουν τον άνθρακα, ο οποίος είναι παρόν και έχει σημαντική συνεισφορά στο προϊόν. Γι' αυτόν τον λόγο αποφασίστηκε να αγνοηθεί ο άνθρακας ώστε τα αποτελέσματα της ελλειψομετρίας να μπορούν να αξιοποιηθούν για τη διαμόρφωση του κινητικού μοντέλου, με το σημαντικό βέβαια σφάλμα που αυτή η απόφαση θα επέφερε.

Τα αποτελέσματα της στερεής φάσης συνοψίζονται στον ακόλουθο πίνακα.

Experiment Code	T (°C)	Deposition rate nm/min	at.%N
TD3	650	0.54	7
TD4	650	0.9	2
TD5	650	0.2	20
TD6	650	0.6	9
TD7	650	0.65	14
TD8	650	0.54	7
TD9	650	0.24	40
TD11	650	0.44	39
TD12	650	0.83	8
TD14	625	0.39	10

Στα αποτελέσματα που παρουσιάζονται συμπεριλαμβάνεται σφάλμα επαναληψιμότητας 7% καθώς και 10% από το μοντέλο της ελλειψομετρίας.

Παράλληλα οι τρεις μέθοδοι ανάλυσης της αέριας φάσης έδωσαν σημαντικές πληροφορίες σχετικά με τις αντιδράσεις που συμβαίνουν στον αντιδραστήρα και είχαν καταλυτικό ρόλο για τη διαμόρφωση του κινητικού μοντέλου.

Οι ενώσεις που ανιχνεύθηκαν στην αέρια φάση από το GC-MS μαζί με τη χημική ρίζα που ανιχνεύθηκε από το ESR οδήγησαν στην πρόταση της αρχικής αντίδρασης που λαμβάνει χώρα στον αντιδραστήρα, η οποία είναι η αποσύνθεση του TDMSA σε δύο ενδιάμεσες ενώσεις.

V1:

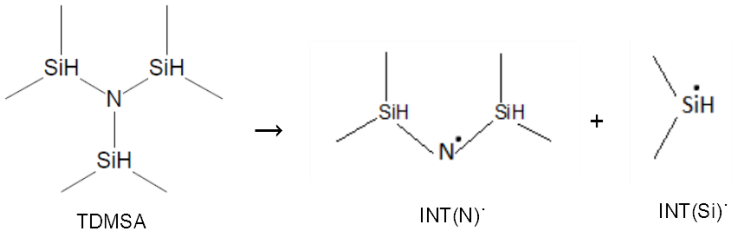

Οι δύο αυτές ενδιάμεσες ενώσεις, σύμφωνα με τον μηχανισμό που προτάθηκε αντιδρούν για την παραγωγή του επιστρώματος μέσω των ακόλουθων αντιδράσεων.

$$\mathbf{S1}:\ \mathbf{I}\mathrm{NT(Si)} + 02 \rightarrow \mathbf{SiO_2}$$

$$\mathbf{S2}:\ 4\mathbf{I}\mathrm{NT(N)} \rightarrow \mathbf{Si}3\mathrm{N}_4$$

Τέλος, απαραίτητη ήταν και η πρόσθεση μιας ακόμα αντίδρασης για τον καλύτερο έλεγχο των αντιδρώντων, συγκεκριμένα του οξυγόνου, και της μιας από τις ενδιάμεσες ενώσεις καθώς και για την εισαγωγή ενός από τα παραπροϊόντα που παρατηρήθηκαν από την ανάλυση της αέριας φάσης.

$$\boldsymbol{V2}:\quad \boldsymbol{3INT(Si)^{\cdot} + 2O_2 \rightarrow Siloxane + H_2O}$$

Οι τέσσερεις αυτές αντιδράσεις αποτέλεσαν τον χημικό μηχανισμό πάνω στον οποίο βασίστηκε το φαινομενικό κινητικό μοντέλο.

Για τη διαμόρφωση αυτού του μοντέλου απαραίτητη ήταν η πραγματοποίηση ορισμένων υπολογισμών σχετικών με τις κινητικές του παραμέτρους. Τέσσερα ήταν τα στοιχεία που έπρεπε να υπολογιστούν πριν την έναρξη των προσομοιώσεων. Οι στοιχειομετρικοί συντελεστές των αντιδράσεων, κάποιες αρχικές τιμές για τον παράγοντα συχνότητας και την ενέργεια ενεργοποίησης, η μετατροπή του TDMSA και η απόδοση του TDMSA. Αυτοί οι υπολογισμοί βοήθησαν στην διαμόρφωση ενός αρχικού κινητικού μοντέλου το οποίο θα βελτιστοποιηθεί μέσω των προσομοιώσεων και την ανατροφοδότηση από την ανάλυση της στερεής φάσης.

Για την πραγματοποίηση των προσομοιώσεων είναι απαραίτητη επίσης η διαμόρφωση του περιβάλλοντός του. Οι προσομοιώσεις πραγματοποιήθηκαν με τη βοήθεια του λογισμικού ANSYS Fluent

18.2. Η γεωμετρία του σωληνοειδούς αντιδραστήρα αναπαραστάθηκε στο λογισμικό με αρκετή ακρίβεια και λόγω ύπαρξης συμμετρίας ήταν δυνατή η εξοικονόμηση υπολογιστικής δύναμης καθώς αναπαραστάθηκε μόνο ο μισός αντιδραστήρας. Το πλέγμα που χρησιμοποιήθηκε χρειάστηκε να μειωθεί σε πυκνότητα από 1.9 εκατομμύρια κελιά που ήταν ο αρχικός του σχεδιασμός σε μόλις 250.000 καθώς η υγειονομική κατάσταση που επέφερε ο COVID-19 κατέστησε αναγκαστικό να λειτουργήσει το λογισμικό από μη επιστημονικό υπολογιστή και συνεπώς έπρεπε να εξοικονομηθεί όσο το δυνατόν περισσότερη υπολογιστική δύναμη.

Τα θερμοκρασιακά προφίλ που χρησιμοποιήθηκαν για τις προσομοιώσεις διαμορφώθηκαν για να ταιριάζουν με τις θερμοκρασιακές βαθμίδες που παρατηρούνται στον αντιδραστήρα. Αυτό επιτεύχθηκε χάρη σε μετρήσεις μέσω θερμοστοιχείων που τοποθετήθηκαν στον αντιδραστήρα και την πολυωνυμική αναγωγή τους σε όλο το μήκος του.

Τέλος, σημειώνεται ότι η μεθοδολογία των προσομοιώσεων είχε σαν στόχο την διαμόρφωση ενός κινητικού μοντέλου ικανού να αναπαραστήσει ένα από τα πειράματα (TD7) και στη συνέχεια το μοντέλο αυτό να δοκιμαστεί και στα υπόλοιπα.

Η διαδικασία των προσομοιώσεων αξιοποίησε όλα τα παραπάνω στοιχεία και μετά από αρκετές προσπάθειες και συνεχείς βελτιστοποιήσεις επιτεύχθηκε το ακόλουθο αποτέλεσμα.

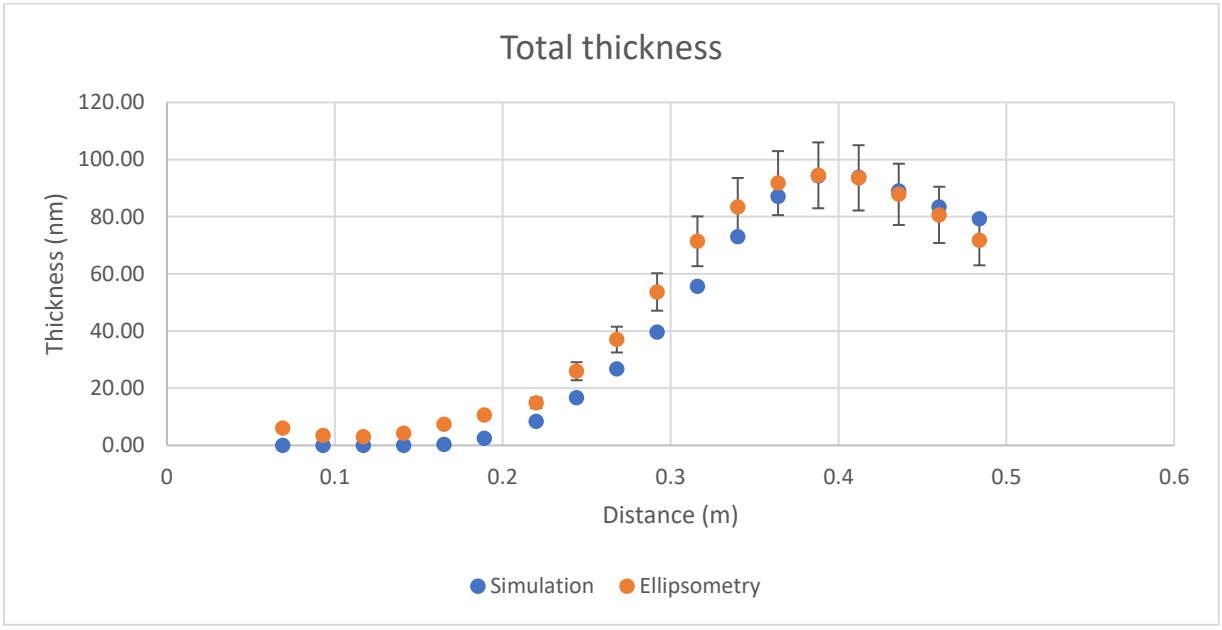

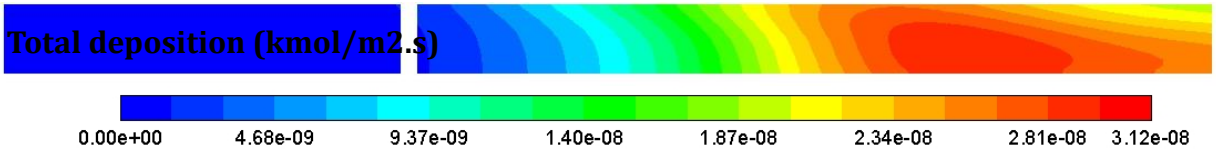

Το κινητικό μοντέλο που διαμορφώθηκε είναι το ακόλουθο.

Kinetic system	Ea (kJ/mol)	A
V1	2.51E+02	1.80E-01
S1	3.00E+08	1.00E+20
S2	4.00E+08	1.20E+19
V2	5.26E+08	7.00E+34
a	**b**	**c**
1.76	0.43	1.2

Στη συνέχεια παρουσιάζονται τα αποτελέσματα και η σύγκριση των πειραματικών και προσομοιωμένων ρυθμών απόθεσης όλων τον προς εξέταση πειραμάτων.

TDMSA = 2sccm	O_2 $(sccm)$	T°C
TD11	0.3	650
TD7	0.6	650
TD12	1.2	650
TD14	0.6	625

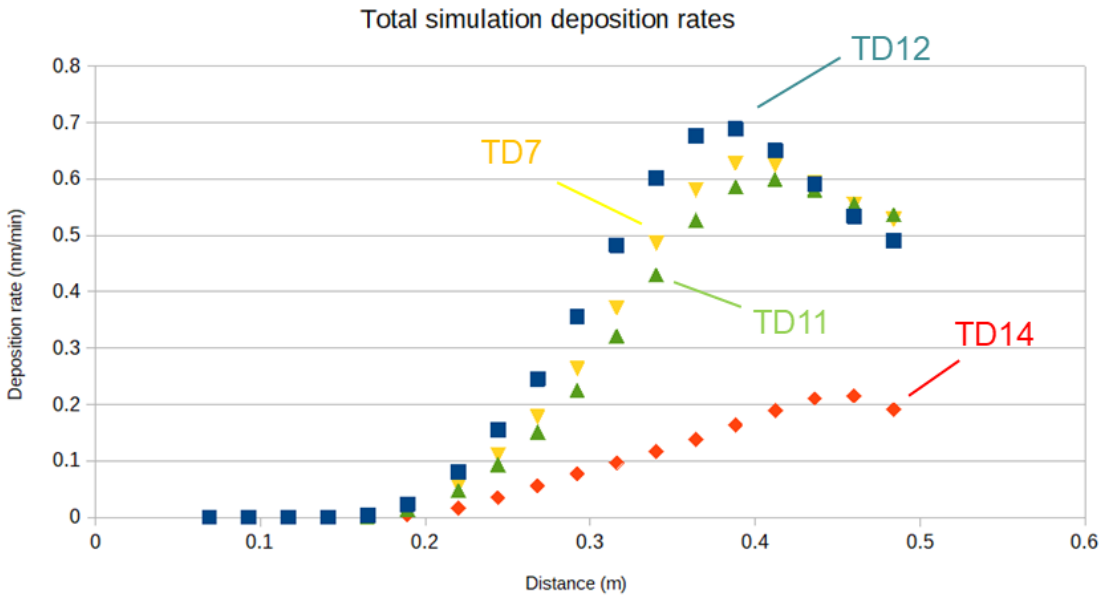

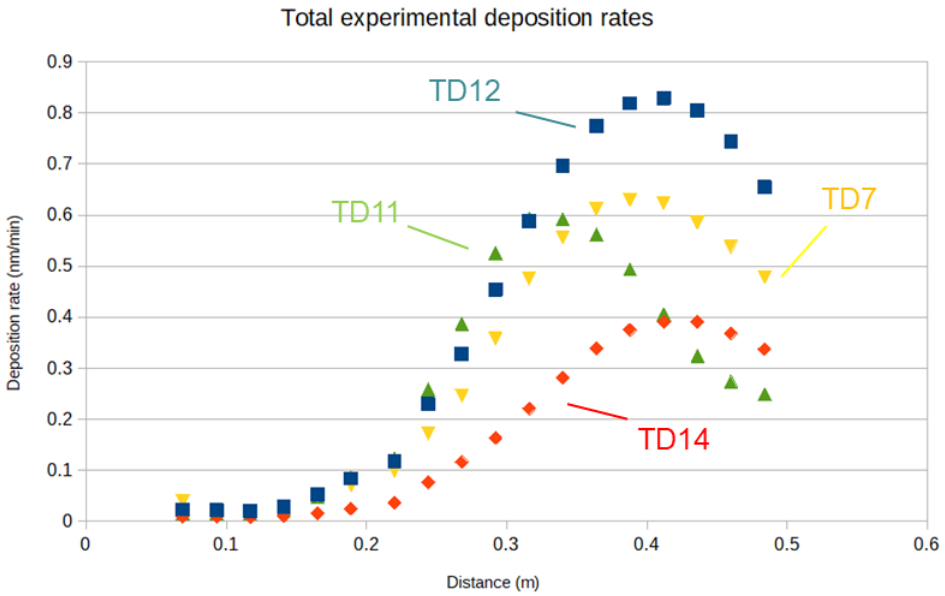

Τέλος παρουσιάζονται τα αποτελέσματα των προσομοιώσεων για το ατομικό ποσοστό αζώτου.

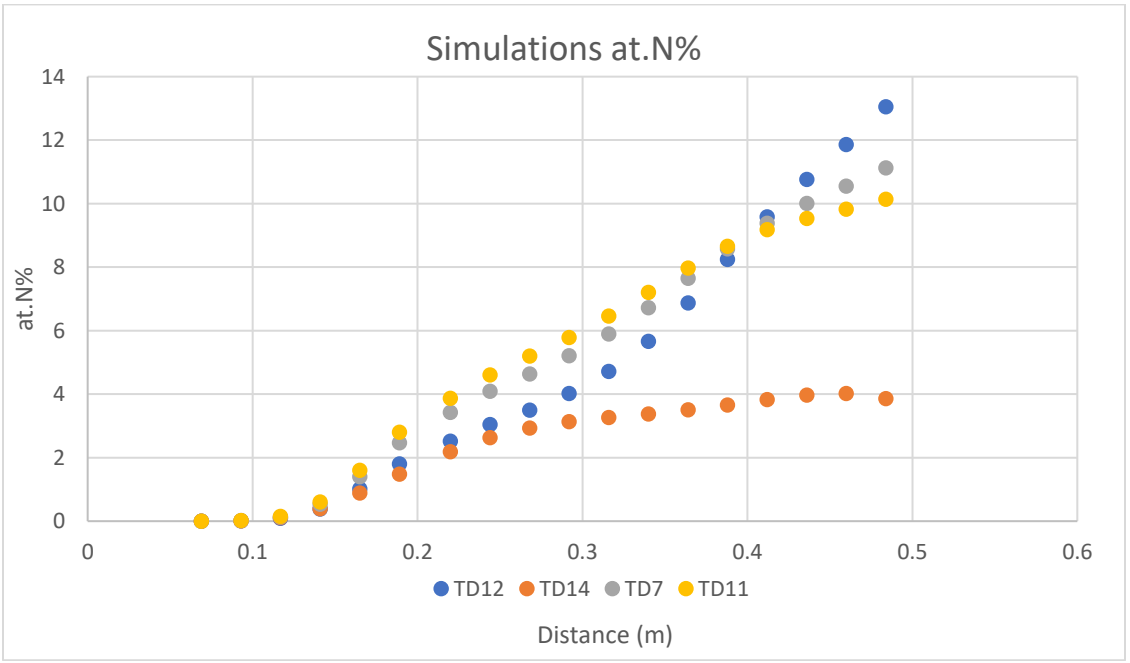

Το συμπέρασμα αυτής της έρευνας είναι ότι αν και τα αποτελέσματα είναι ικανοποιητικά, η παραδοχή της αγνόησης του άνθρακα επιφέρει σημαντικό σφάλμα. Σε περίπτωση βέβαια της ύπαρξης αξιόπιστων δεδομένων για τον άνθρακα στη δομή του επιστρώματος, και με την κατάλληλη μεθοδολογία η έρευνα αυτή θα μπορούσε να γίνει ακόμα πιο συμπαγής.

Λέξεις κλειδιά: Computational Fluid Dynamics, Χημική απόθεση ατμών, οξυνιτρίδια του πυριτίου, προσομοίωση, κινητικό μοντέλο, ανάλυση αέριας φάσης

Table of contents

Nomenclature

Symbols:

A_0	Pre-exponential factor (s^{-1})
a, b, c	Partial order exponents a, b, c
at.N%	Atomic Nitrogen percentage (%)
C	Concentration ($kmol.m^{-3}$)
E_a	Activation energy ($J.kmol^{-1}$)
k	Reaction rate coefficient
L	Length of the reactor (m)
P	Pressure (Torr)
Q	mass flow ($kg.s^{-1}$)
R	Universal gas constant ($J\ mol^{-1}\ K^{-1}$)
r	Rate of the reaction ($kmol.m^{-3}.\ s^{-1}$ or $kmol.m^{-2}.s^{-1}$)
S	Surface area (m^2)
T	Temperature (°C or K)
V	Volume (m^3)
X	Conversion (%)

Subscripts:

i	(on) sample i
in	inlet
out	outlet
r	chemical reaction r

Abbreviations:

CFD	**C**omputational **F**luid **D**ynamics
CVD	**C**hemical **V**apor **D**eposition
ESR	**E**lectron **S**pin **R**esonance spectrometry
FTIR	**F**ourier **T**ransformation **I**nfrared **S**pectroscopy
GC-MS	**G**as **C**hromatography – **M**ass **S**pectrometry
HTCVD	**H**igh **T**emperature **CVD**
INT	Fictive group of reactive **int**ermediate compounds
NMR	**N**uclear **M**agnetic **R**esonance
PFR	**P**lug **F**low **R**eactor
sccm	**S**tandard **C**ubic **C**entimeters per **M**inute, a unit of volumetric flow
TDMSA	**T**ris **Dim**ethyl**s**ilyl **A**mine
UDF	**U**ser-**D**efined **F**unction

Chapter 1 Introduction

1.1 Project Objectives

The present thesis was conducted as part of the research done for the HEALTHGLASS project, sponsored by the Agence nationale de la recherché (ANR). The goal of the HEALTHGLASS project is to develop new CVD processes for the deposition of SiO_2, SiO_xC_y and SiO_xN_y thin films at relatively low temperatures (T<570 °C) on thermosensitive substrates such as glass or plastic. The current report, being the result of a work linked with the deposition and process simulation part of the project, will deal exclusively with the production of the amorphous SiO_xN_ythin films, and the development of a chemical model able to reproduce the experimental results in a simulations environment. As such, material characterization and performance results will not be addressed or discussed, since only the material will be studied only from a computational and process aspect.

There is limited information in the literature on the deposition of SiO_xC_y and SiO_xN_y films in respect to the specifications defined by the project, namely the moderately low deposition temperature and the desire to scale-up the process in industrial scale, which requires therefore an atmospheric pressure based process. These specifications dictate certain limitations, which impact the choice for the most suitable CVD process, one which namely can combine deposition under atmospheric pressure and at relatively low temperatures. Lastly, based on these constraints, the deposition of dense and chemically inert films with sufficient growth rates is targeted. However, creating a SiO_xN_y film at such low temperatures without the use of a plasma process, which is usually very costly and requires vacuum conditions, is very innovative and ambitious.

Project HEALTHYGLASS aims to achieve this goal, by also establishing process, structure, properties and performance correlations, which will lead to outstanding progress at a fundamental level and will pave the way towards the application of these multifunctional and durable materials in complementary sectors concerned by the functionalization of complex surfaces such as micro- and nano-electronics, plastics, medical devices and implants, or gas sensors.

1.2 Work environment

The present thesis was done based on research conducted at the École Nationale Supérieure des Ingénieurs en Arts Chimiques et Technologiques (ENSIACET) of the Institut National Polytechnique de Toulouse (INPT), in Toulouse, France. It is a cooperation between the National Technical University of Athens (NTUA) and INPT through the ERASMUS+ program.

ENSIACET houses many laboratories, two of which are the Laboratoire de Génie Chimique (LGC) and the Centre Inter-universitaire de Recherche et d'Ingénierie des Matériaux (CIRIMAT). The internship was performed at LGC, with frequent meetings held between members of both laboratories, collaborating as partners under the umbrella of the HEALTHGLASS project.

LGC's boarder research is on the field of Chemical Engineering and the laboratory consists of six departments, each focusing on different aspects of the same field. The common goal is to design, operate, optimize and scale-up a wide range of processes, some of which membrane, electro-, and bio-processes, etc. [1]

The department responsible for this thesis on the side of the LGC laboratory is the Ingénierie des Réacteurs Polyphasiques Innovants (IRPI). This group generally focuses on designing multi-phase reactors, involving the combination of three general themes: catalytic reactor engineering, activation and oxidation processes, and fluidization and CVD process engineering. [2] The current work falls under the "Fluidisation and CVD Process Engineering" category and focuses specifically on the computational part of the process.

The CIRIMAT laboratory is centered around research conducted in the field of Science and Materials Engineering. Similarly to LGC, it consists of various research groups, each of them carrying out work in one of the following fields: material science, nanomaterials engineering, coatings and deposition processes, and ageing and durability of materials. The interest in these fields is vast and affects many different areas of work and industry sectors, including aeronautics, energy, health industry, and others. [3]

The CIRIMAT-INP department collaborating with LGC in the frame of project HEALTHGLASS is SURF: Surfaces: Réactivité-Protection. This department has as a main activity the surface reactivity and protection which can be further expanded into three separate, but interconnected activities: implementing CVD processes for the deposition of protective coatings, characterizations of the deposited films, and modelling the film growth stages. [4]

Apart from the LGC and CIRIMAT laboratories at INP, additional laboratories are collaborating in this project, each providing their respective expertise. These partners are:

CIRIMAT UPS: precursor chemistry, mechanical properties, gas phase analysis
CEMHTI: solid phase characterizations
Industrial partner: Feedback and material performance using standard industry testing protocols

The thesis was organized in the frame of an ongoing PhD thesis, assigned to the PhD student K.C. Topka, working both on the experimental and simulation aspects of the CVD of SiO_xN_y and SiO_xC_y thin films into LGC and CIRIMAT. An engineer from CIRIMAT, L. Decosterd, was in charge of the gas phase analyses by Gas Chromatography- Mass spectroscopy (GC-MS), Nuclear Magnetic Resonance (NMR) and Electron Spin Resonance (ESR). Another thesis was devoted to the solid phase analysis through Ellipsometry and Fourier-Transform Infrared Spectroscopy (FTIR). A post-doc researcher was involved in the project researching the mechanical properties of the material developed in the lab, being assisted by another student performing a master internship.

1.3 Scope of this work

In this large and complex project, the goals and responsibilities of each group have been well defined, put on schedule and regularly monitored. This work detailed in the present thesis has been a contribution to the entirety of the project dealing with a part of it, the formation of SiO_xN_y thin amorphous film through CVD processes using TDMSA (tris dimethylsilyl amine, $N(SiH(CH_3)_2)_3$) as the silicon-containing precursor, and O_2 as the oxidant.
The TDMSA precursor was selected to be as both the silicon and nitrogen providing molecule for the SiO_xN_y films that are being researched, and has the following chemical formula. (Fig 1.)

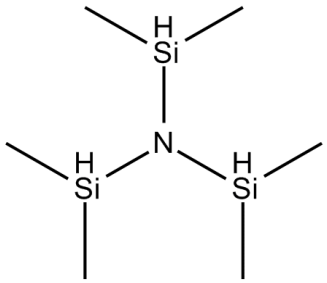

Figure 1. Chemical structure of the TDMSA precursor.

TDMSA was selected to undertake this work since it belongs in the silyl-amine family and contains both silicon and nitrogen atoms. Conventionally, silane (SiH_4) or silazane precursors such as hexamethydisilazane (HMDS) are used for the production of silicon nitride, carbonitride and oxynitride materials, with addition of ammonia in the gas phase. However, the temperatures required for such chemistries to lead to film formation are usually high. It has been shown in the literature that in the case of HMDS, the bonding of the silicon atom to methyl groups renders the molecule more stable and leads as such to a higher temperature required for nitride deposition. It has been argued though that the presence of Si-H bonds instead of Si-CH3 bonds can lower the required temperature for precursor activation. For that reason, the TDMSA precursor was chosen, which so far has only been reported in PECVD patents. The present work is the first time in the literature that the TDMSA precursor has been tested for the production of silicon oxynitrides in the absence of ammonia.

This work has two objectives. The first one deals with combining experimental solid phase and gas phase analysis results in order to correlate and extract information with the aim of developing an apparent but fitting reaction mechanism that can be justified from both experiments and literature finds. The second objective concerns the reproduction of the experimental results in a simulation environment. The proposed mechanism is implemented into the CFD software Ansys FLUENT 18.2 in an effort to recreate the conditions and results of our experiments with ultimately the goal of process optimization. Throughout all this, the experimental aspects are to a certain extent, defined and modified through the constant feedback of the solid and gas phase analysis.

1.4 Structure of the thesis

At this part a bit more light will be shed on the structure of this work and subsequently on the structure of this thesis since it has been put together in a way that resembles the work flow followed during the conducted research.

The research of the present subject begun with studying the chemical system that has been selected, and more specifically the $TDMSA/O_2$ chemical system. The first step was to create a kinetic model for this system that is coherent with the gas phase and solid phase analyses and the literature finds. Once this apparent kinetic model takes its form, we need to suggest experiments and utilize the experimental results in order to obtain information, such as the kinetic parameters of the reactions suggested.

After having extracted all potentially useful information from the experiments, the computational processes begun using the aforementioned simulation software. Once the computational environment is created and the assumptions are set, the simulations can begin. Step by step the reactions suggested for the kinetic model are implemented in a coordination of calculations and manual fitting, seeking for results that agree with the experiments.
The simulation process is aimed in fitting one of the experiments and confirming the application of the developed kinetic model in the other experimental runs, which lead to further information on its improvement and optimization.
Final point of the simulation process is of course the optimization of the deposition process, by utilizing the potential of the chemical system, and finding the optimal deposition conditions that will give the highest output/yield and the most uniform deposit thickness on the industrial substrates of interest.

In this thesis, the experiments taken place in the CVD reactor and the analysis of their solid and gas phase results are briefly discussed. The proposed apparent chemical mechanism and the associated kinetic laws are detailed and justified and finally this report will go into the simulations starting by its architecture and foundations and moving towards the results of the attempts to simulate the reality of the reactor.

Chapter 2 Literature Review

2.1 Theoretical background on thermal CVD processes of SiO_xN_y thin films and its CFD simulations

The main part of this work that addresses the research of low-temperature formation of SiO_xN_y films through thermal CVD processes at moderately is a very novel work with very little scientific representation. For this reason, the literature search has been a difficult task throughout this thesis, especially for processes that do not rely on plasma utilization. Having said that, the CVD processes themselves on the contrary are very well studied and are additionally well known within the scientific community. The literature search that has occurred during this thesis, due to the lack of scientific papers pertaining to these specific precursors, had to often drift onto molecules with similar chemical structure. Based on this literature, an overall opinion on what we could expect from the studied TDMSA compound could be formed, and experimental parameters such as gas flows and potential deposition temperatures could be limited down to specific ranges.

Silicon oxynitride (SiO_xN_y) is an important inorganic material widely studied for its outstanding electronic and mechanical performance. SiO_xN_y is the intermediate phase between silicon dioxide (SiO_2) and silicon nitride (Si_3N_4), which possesses high durability at high temperature, high resistance to thermal-shock and oxidation, high density, excellent mechanical performance, and a low dielectric constant [7]. Due to these unique performances, SiO_xN_y has great potential for high-temperature related applications, for example, it is typically used in non-linear optics and as mechanical component owing to its high strength, thermal insulation, and electronic and chemical resistance. SiO_xN_y is additionally attractive in integrated circuits (IC), barrier layers, non-volatile memory, optical waveguides, organic light emitting diode (OLED), and anti-scratch coatings applications. [7]

SiO_xN_y films can have an adjustable dielectric constant, refractive index, and extinction coefficient by controlling the ratio of nitrogen/oxygen in the chemical composition. The ratio of the reactive gases, as well as other process parameters involved in the preparation of SiO_xN_y are important in tuning the stoichiometry of each element in the produced $SiO_xN_y$is material. As shown below (Fig.2), a series of possible forms of the SiO_xN_y can be found, ranging between pure silicon dioxide, to pure silicon nitride, and silicon rich variations. The composition of the material changes as the properties of the film, based on the N and H content increase or decrease. The main properties affected are changes in transparency, band gap width, refractive index, and insulation.

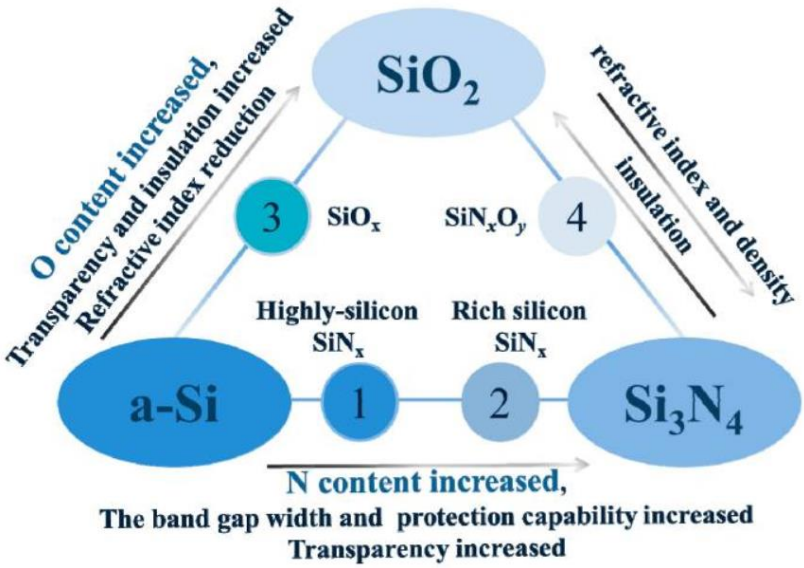

Figure 2. Properties of SiO_xN_y materials [7].

A SiO_xN_y film generally has a performance between SiO_2 and Si_3N_4. Due to its excellent photoelectric performance, it has been widely used in optical devices, dielectric gate dielectric materials, and optical waveguide materials. The SiO_xN_y film also has high chemical stability, high resistance to impurity diffusion, and water vapor permeability, which renders it a very promising material for applications in barrier devices such as gas barriers. In addition to that, SiO_xN_y films have a small defect density and are advantageous in applications as a potential storage medium. [7]

For the deposition of thin SiO_xN_y films, the chemical vapor deposition process presents major advantages, explaining why it is used since several decades for thin film deposition. During the growth of thin films, the preferred precursor is transported into the reaction chamber in the form of vapors. Inside the reaction chamber, the substrate to be coated is kept to a desired temperature, which enables the reactive gas molecules to decompose onto the substrate and yield film deposition. Depending on the experimental conditions, the deposited film may be in amorphous or polycrystalline in nature. [6] CVD based technics are mainly divided into plasma enhanced CVD (PECVD), low-pressure CVD (LPCVD), photochemical vapor deposition, thermal CVD, etc. Among them, PECVD and LPCVD are the most employed processes. [7]

For the formation of SiO_xN_y a variety of different CVD processes has been reported in the literature, each having distinct advantages, and disadvantages. A brief table with the characteristics of the main CVD processes is presented below.

Table 1. Comparison of various CVD processes for the production of silicon oxynitrides. [7]

Method	Advantages	Disadvantages
PECVD	Flexible operation method, High process repeatability, High step coverage, Low deposition temperature (<400 °C)	High cost, High H content in film
LPCVD	Uniform film, Complete structure, Less pinhole defects, High deposition speed, Large-area preparation	Low heating rate, Long reaction time, High deposition temperature (generally >550 °C)
HTCVD	Simple operation and operation, High reaction rate, Low H content in film and dense structure	High deformation, Impaired interface performance
Photo-CVD	Low reaction temperature (≤250 °C), Smooth film surface, Less by-products	High cost, Low film stability

Computational fluid dynamics (CFD) models for CVD reactors are of high importance, since they help significantly in optimizing the deposition process. With the aid of CFD models we can simulate the local gas phase composition, temperature profile and reactor geometry, and as such extract information on species concentration profiles, and local deposition rates on parts of the reactor that would otherwise be difficult to measure experimentally. When being supplied by constant feedback from the experimental results, simulation is a powerful tool for optimizing the geometry and the deposition conditions that lead to the desired film thickness and composition. This constant feedback is even more important in complex systems and it gives the opportunity to link different process parameters with each other. [8]

The way the kinetic model of the CFD is constructed is almost always through an “apparent mechanism”. Described as an apparent mechanism is a kinetic model that only provides a simplified but precise enough vision of the reality of the reactor, leaving aside unnecessary complexities. Its goal is the general description of the system in order to be represented into a CFD software.

In CVD the construction of such a mechanism requires data from the experiments. The solid phase analysis is always present in the development of such a mechanism and it provides important information on the formation of the films. A gas phase analysis is used frequently, however it can be also of high significance since it can provide qualitative and quantitative information on the by-products of a CVD process. This information, in accordance with literature finds, will give the researcher the necessary insight to suggest a number of potential reactions that take place within the reactor for the studied chemical system. These proposed reactions may have assumed intermediates and kinetic parameters, as long as their assumption is based on realistic hypotheses which, after implementation into a computational software, can recreate the experimental results in a satisfactory manner. That means that even though our mechanism for the biggest part is simplified, it needs to have its foundation strongly linked to experimental results. The created kinetic model must therefore be constantly tuned in accordance with the new experimental results, keeping the two in a consistent feedback loop.

Chapter 3 Materials and Methods

3.1 Experimental process

The experiments were performed in a horizontal, tubular, hot-wall reactor (Fig.3) configuration described in more detail in an already published work [5]. This reactor is constructed by a fused silica tube with an inner diameter of 46 mm and a length of 700 mm. The heating of the reactor happens through its walls by a semitransparent furnace (Trans Temp, Thermcraft Inc.) and the wall's temperature profile is measured every 20 mm along the tube using a type-K thermocouple with an accuracy of ±2°C. The experiments were performed at two different set point (SP) temperatures, namely 650, 625°C, defined as the temperature measured at 360 mm from the inlet, after which a 140 mm long isothermal region exists. Before 360 mm, axial thermal gradients were present and measured as detailed later.

The reactor's base and operating pressures were monitored with a Pirani (MKS MicroPirani Transducer Series 925C) and a Baratron (MKS Baratron Type 627) gauges respectively, positioned downstream of the deposition zone, before a liquid nitrogen trap and a dry pump (Edwards, soXu 20iC). The operating pressure was fixed at 97.3 kPa (730 Torr) for all runs.

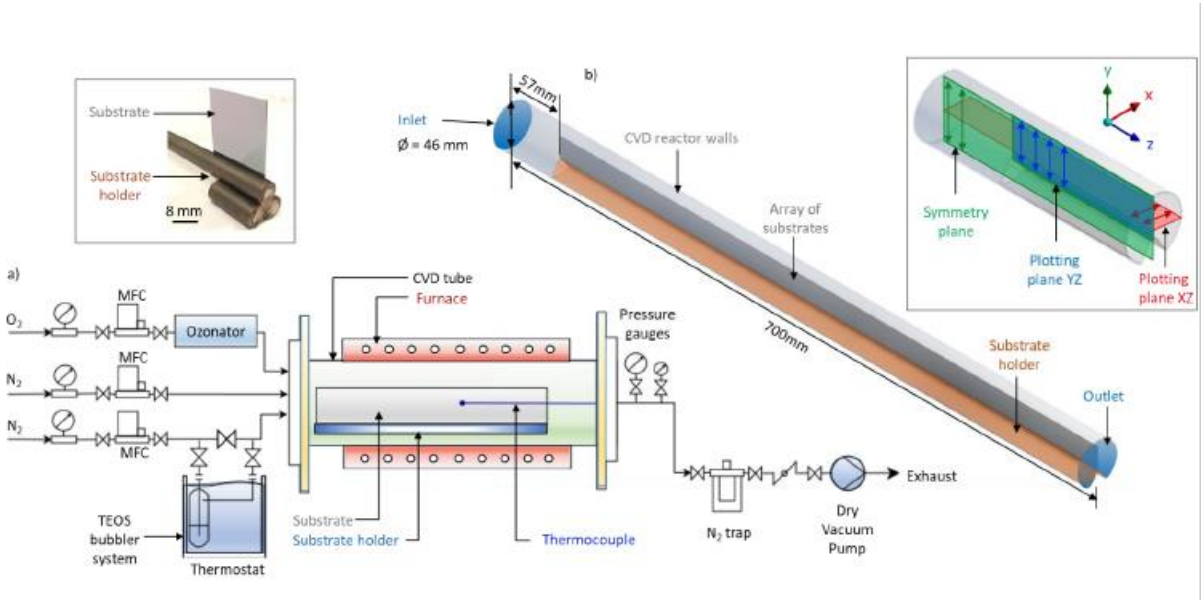

Figure 3. Tubular reactor. Schematic (a) and 3D (b) representation of the CVD reactor (not true-to-size and proportion). Top left inset photograph shows the substrate holder supporting a Si coupon vertically. Top right inset scheme depicts the symmetry plane, the plotting plane YZ used for surface results presentation and the plotting plane XZ used to present gas phase results [5]

For the deposition, 280 μm thick monocrystalline silicon (100) wafers (Neyco) (Fig.4) were cut in rectangles of 32×24 mm2 and used as substrates. Before being inserted into the reactor, the substrates were degreased in a succession of three ultrasound bath steps, including: 1) an ultrasound bath using distilled water for 5 min, then rinsed with acetone, 2) an ultrasound bath using acetone (>99%, VWR

Chemicals) for 5 min, then rinsed with ethanol, 3) an ultrasound bath using ethanol (99.3%, VWR Chemicals) for 5 min, and finally dried under Ar (99.9999%, Messer) flow.

Within the reactor, the substrates were supported vertically by home-made, tubular, stainless steel substrate holders, with a 7 mm deep insertion slot, positioned on the row. Their total length was 450 mm, supporting a maximum of 18 coupons for each run. The first substrate was placed at 57 mm from the reactor inlet.

Figure 4. Placement and arrangement of the 18 samples on the stainless-steel sample holders.

Figure 5. Photograph of a stainless-steel sample holder.

Several CVD experiments were conducted in the laboratory reactor performed by K.C. Topka. The conditions of all the experiments are summarized in Table 2.

Table 2. Experimental conditions of the performed experiments using TDMSA.

Experiment Code	T (°C)	TDMSA $flow\ rate$ (sccm)	$O_2\ flow\ rate$ (sccm)	$NH_3\ flow\ rate$ (sccm)
TD3	650	6	0.6	40
TD4	650	2	2	20
TD5	650	2	0	20
TD6	650	2	0.6	20
TD7	650	2	0.6	0
TD8	650	2	0.6	40
TD9	650	2	0	0
TD11	650	2	0.3	0
TD12	650	2	0.6	0
TD14	625	2	1.2	0

The starting chemistry tested was a $TDMSA + O_2 + NH_3$ chemistry. Through carefully selected experiments and parametric analysis of this chemistry, it was concluded that the presence of NH_3 does not contribute to the SiO_xN_y deposition at the tested temperature range, and additionally has negative effects on both the deposition rate and the nitrogen content of the films (results are part of a different thesis and are therefore omitted). Thus, the decision was made to exclude ammonia from the chemistry and investigate the $TDMSA + O_2$ system. For this reason, a set of parametric analysis that investigated the effect of the oxygen flow rate was done through experiments TD7, TD9, TD11, TD12 and TD14 of Table 2. The starting experiment for which the simulations were constructed on was TD7, utilizing information from all other experiments. The NH_3 containing experiments had mainly a supportive role, in terms of formed gas phase by-products, but where not considered for the simulation process itself.

3.2 Solid phase analysis

The analysis of the solid phase is the foundation of the development of the kinetic system. The Master intern, Paris Papavasileiou performing these analyses had in his disposal two methods, Reflective Ellipsometry and Fourier Transformation Infrared Spectroscopy (FTIR).

FTIR of solid films is a non-destructive method using the molecule vibration under light absorption as its main principle to produce results. FTIR for the most part is trying to give information on the structure of the film and on the bonds between the atoms that exist within it. In combination with ellipsometry and the gas phase analysis results, it was able to provide us with information about the bonds and the structure of the film, which was necessary for suggesting an apparent deposition mechanism.

Reflective Ellipsometry is a non-destructive method that enables the measurement of the produced films' optical properties, from which secondary information such as film thickness, composition and density can be extracted, among others. In the present study, Reflective Ellipsometry was utilized to provide information on the thickness of the films, as well as a first estimation of its atomic Nitrogen content, by

simulating a SiO_xN_y material, represented by two homogeneously mixed phases, namely amorphous SiO_2 and Si_3N_4.
In more detail, the film, which is composed of varying atomic percentages of Si, O, C, N and H, was represented in a simplified way as a homogeneously mixed two-phase material. This way, separating the film into two layers through the volumetric fraction of each phase, allowed for a satisfactory and fast approximation of the nitrogen content, and the hypothetical thickness of each phase.

Additionally, the samples were always weighted before and after the experiments, but the weight difference could only give a general idea on the thickness of the samples since there was a significant fluctuation of thickness on each sample. Therefore, most of the information regarding the deposition rates and the thickness of each sample, were taken by the local measurements of ellipsometry, which were probed on 5 different probes along the vertical center of each sample, and then averaged.

The film created by the $TDMSA/O_2$ chemical system is an amorphous $SiO_xN_yC_zH_a$ thin film. The model suggested by ellipsometry though, does not give information of the carbon and hydrogen content. Through the IBA analysis that were performed on various samples into CEHMTI, it was observed that carbon has an important influence in the formation of the film. As the health situation related to COVID-19 impeded the work progress in relation to the IBA analyses, we were obliged to follow the two-phase model of ellipsometry, even if we knew that it led to an important error on the estimation of the films' composition. Despite that, until a new model that considers carbon is proposed and verified, the kinetic model we developed during the internship is a simplified two-phase model:

$$SiO_2 + Si_3N_4 \rightarrow SiO_xN_y$$

3.3 Gas phase analysis

Through the efforts of the collaborating partners at CIRIMAT-UPS, the project had the rare opportunity to include an extensive gas phase analysis of the CVD process. The information provided by the three gas-phase analysis techniques was a great aid in the development of the kinetic model. Qualitative results of the stable and radical gas-phase by-products, as well as the overall gaseous composition at the exit of the reactor can provide information on the reactions occurring during deposition. In parallel, the quantitative results on the TDMSA conversion rate can help us calculate some kinetic parameters that will be later implemented in the simulations.

The three methods used for the gas face analysis were: Electron Spin Resonance spectrometry (ESR), Gas Chromatography – Mass Spectrometry (GC-MS) and Nuclear Magnetic Resonance (NMR). GC-MS and NMR were used to identify the stable by-products existing in the gas phase, while the ESR method was used to identify potential radical species that are very reactive and thus hard to observe.

For this reason, the ESR requires the use of a spin-trap, namely a molecular that can trap radical species and stabilize them for analysis. The compound POBN is used for this purpose (Fig. 6).

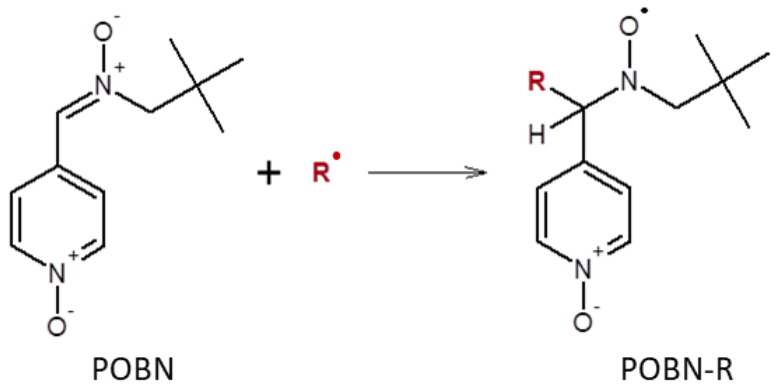

Figure 6. POBN compound used for the ESR characterization method.

Through this analysis, we were able to identify radical species that are potentially the building blocks of the chemical mechanism.

At the same time, GC-MS and NMR give information on the by-products that exit the reactor. This analysis can give both qualitative and quantitative results, although in our case the results were mostly qualitative due to time constraints related to the global health situation.

These two methods in combination can give a great amount on information on what is happening inside the reactor and thus helping us construct the kinetic model.

3.4 CFD modeling

To represent the deposition rate and the reactive transport phenomena taking place in the CVD reactor a CFD model was constructed. This model is taking into consideration the gas phase and surface chemical reactions that are suggested by the apparent chemical model constructed. The local gas flow and temperature profiles in the reactor were calculated by solving the mass and momentum conservation and thermal energy balance equations in each elementary discretized volume. The local distribution of species mass fractions and deposition rates were calculated after considering the kinetic data of the homogeneous and heterogeneous reactions into the species conservation equations. The software utilized to produce the numerical simulations is ANSYS® FLUENT® 18.2, with a cell-centered finite volume scheme and second-order spatial accuracy.

3.4.1 FLUENT environment

In this part the modeling and the building blocks of this simulation will be justified. It should be mentioned that the mesh and geometry for these simulations where made and optimized in a previous thesis by George Alexander Chliavoras, graduate of the NTUA school, working on this project with K. C. Topka, and for this reason these aspects of this work will only be mentioned briefly.

3.4.2 Geometry

The geometry implemented in FLUENT has been designed to be as close as possible to the actual geometry of the reactor. All these elements have been considered and represented when creating the geometry of the reactor.
It must be mentioned that while the tubular reactor has a shape which is easily replicated in a simulation environment, the particular geometry of the sample holders and arrangement of the samples themselves made this task considerably more difficult.
All dimensions were kept true to the original size, except from slight simplifications made to the sample holder geometry. The tubular reactor was represented as a half cylinder, cut along the YZ-plane with a rounded-up version of the sample holder represented through most of the reactor's length.

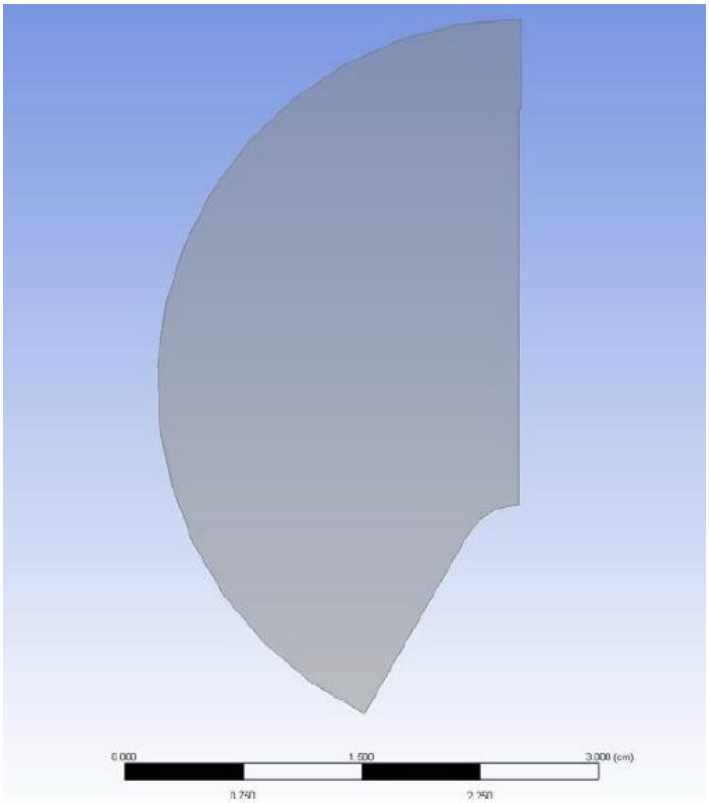

Figure 7. Cross-section of the flow domain of the simplified tubular reactor, in the area of the substrate. [5]

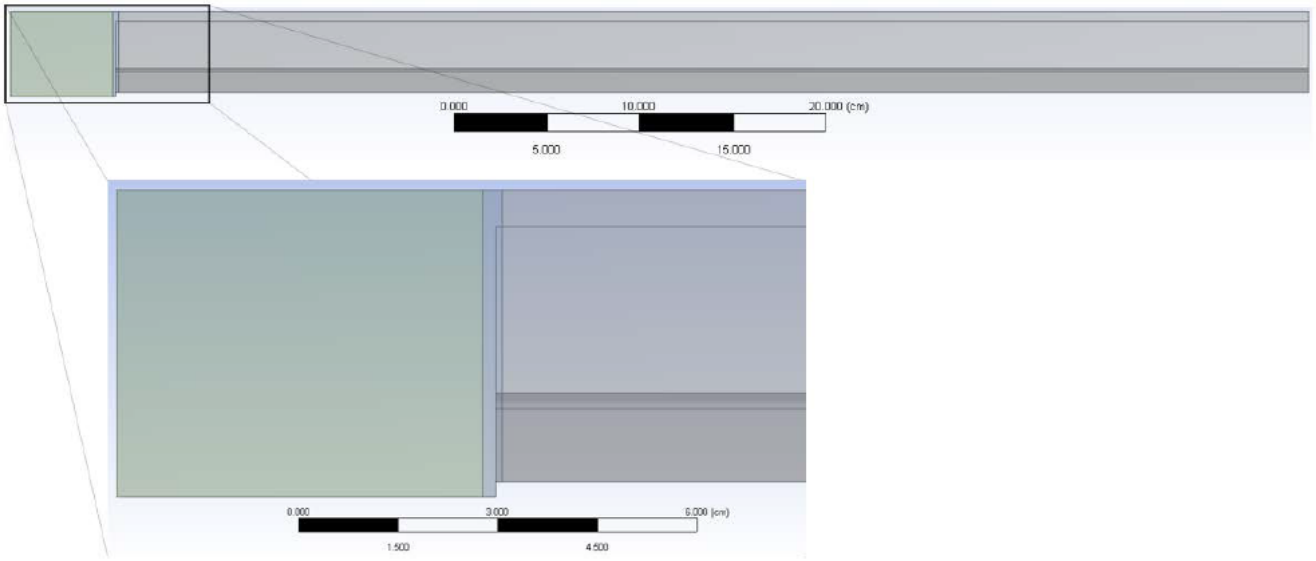

Figure 8. Modeled tubular reactor flow domain geometry. The three meshing segments can be seen: inlet (left), outlet (right), and transitional (thin slice in between). [5]

The symmetry existing on the reactor which allows us to make simulations on a geometry that represents just half of the actual reactor has an important role since it can save a lot of computational power and thus time.

3.4.3 Mesh

The construction of the mesh, similar to the geometry, was made harder because the existence of the sample holder at only parts of the reactor, a feature led us to splitting the geometry into three different meshes.

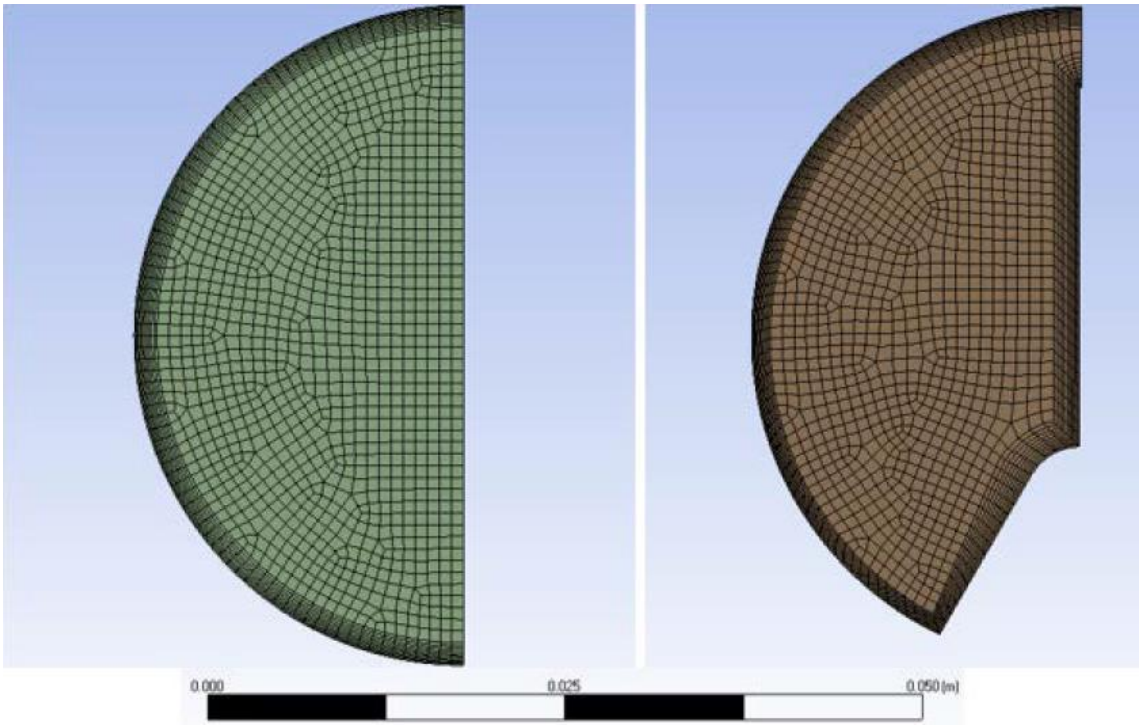

Figure 9. Tubular reactor mesh: Inlet (left) and outlet (right). [5]

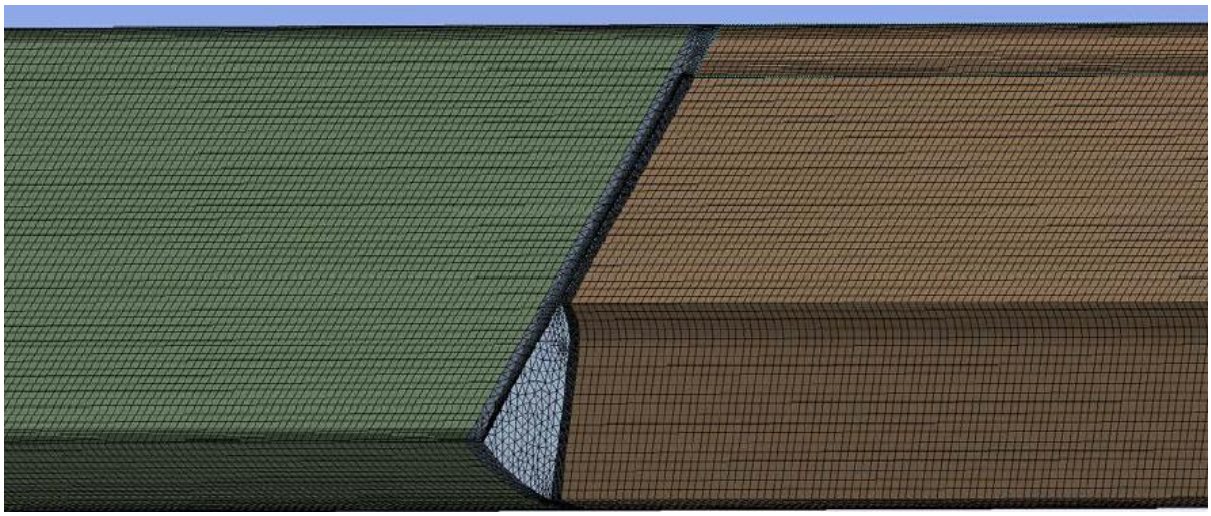

Figure 10. Tubular reactor mesh: the three segments.

Different sizes of meshes have been created for different purposes. All of these meshes share the same characteristics but differ only in the number of cells. The most important principle behind designing the mesh is that the mesh is more refined close to all the walls of the reactor in order to better model the concentration gradients that exist in between every solid surface and the body of the gas. The reasoning behind the different meshes is a matter of computational power. The actual mesh that is run in the laboratory computer consists of 1.9 million cells with a maximum cell size of 0.85 nm. However, due to

the imposed confinement, the simulations had to be run locally at home, on non-scientific computers with low calculation power. Therefore, the number of cells had to be dropped down to decrease the computational strain on the machine and the over calculation time. For this reason, two more meshes were created, having the same architecture with the actual mesh, but with fewer cells, 250.000 and 500.000 to be more precise. The results shown in the current work were extracted from simulations run with the mesh consisting of 250.000 cells and maximum cell size of 0.85mm.

3.4.4 Assumptions and Boundary conditions

The simulations require a series of assumptions that the software will take into consideration. The assumptions presented are implemented to simplify the numerical complexity of the system.

- Pressure based model (P = constant at 97325 Pascal)
- Activated gravity
- Steady state
- Laminar gas flow (Reynolds number < 1000)
- Incompressible gas flow
- Heats of reactions not activated
- Ideal gas

The boundary conditions of the systems are described below:

- A flat profile was considered for the gas velocity at the gas inlet.
- The total mass flow rate, and all species' mass fractions were fixed to the values calculated from the experiments.
- The temperature of the gas at the inlet was set equal to the experimentally measured temperature of the wall close to the inlet.
- A symmetry boundary condition was applied at the YZ symmetry plane.
- A classical no-slip condition was imposed for the gas velocity on all the solid surfaces, the reactor walls, the substrate holder, and the substrates themselves.
- The temperature of the surfaces was set equal to the temperature profile measured experimentally on the reactor walls before deposition, through the implementation of a custom user-defined function.
- In order to avoid backflow in the computations and to speed up convergence a constant temperature was applied for the last 100 mm of the reactor, i.e. between 600 and 700 mm, and the outlet boundary condition was set to "outflow".
- Modifying the temperature profile in this region does not impact the results, since the samples were placed only between 57 and 500 mm from the reactor inlet.
- The mass flux density of each species near the solid surfaces was assumed to be equal to the corresponding heterogeneous reaction rate.
- The total pressure was fixed at the operating pressure.

- A zero-diffusion flux was fixed for all gas phase variables at the reactor exit.
- All reactions were set as forward reactions

The way the experimental results were correlated to the ones of the simulations was through creating user-defined planes within the reactor geometry, representing the 18 samples, or to be more accurate, the part of the samples not covered by the sample holder. The software was able to calculate all the needed parameters of these planes through an area weighted average. Therefore, the simulated deposition rate of each sample could be extracted this way and directly compared to the average results from ellipsometry.

The chemical reaction rates were implemented into FLUENT® in the form of an Arrhenius type expression:

$$r_r = A_{0,r} * \exp\left(-\frac{E_a^r}{RT}\right) * \Pi_{i=1}^{i=n} p_i^a \quad (1)$$

Chapter 4 Results

4.1 Experimental results

4.1.1 Temperature profiles

In order to have an accurate temperature profile for the simulation a series of manipulations is necessary. From the experiments, we obtain a thermal profile, which is then implemented into FLUENT through a UDF (user defined function) by expressing the measured data through polynomial equations. This way our simulation has the same temperature profile and gradient as the experiments.

For each thermal profile, a series of temperature measurements were made on the reactor walls, across the length of the reactor, specifically every 2 cm. To make these measurements the reactor must operate under steady-flow conditions of O_2 and N_2, the carrier gas, but without the influence of the TDMSA since a non-reacting flow is necessary.

Two different thermal profiles were used in this work. The main one being at a set point of $T = 650°C$ and the second one, used for the experiment at lower temperature, at a set point of $T = 625°C$. For each thermal profile, numerous temperature measurements were made across the length of the reactor (along its z-axis). The measurements were then interpolated using 3rd and 4th order polynomials, to express the wall temperature for each profile as a function of the Z-axis. This way, we were able to apply a specific temperature profile on the walls, the samples, and the sample holder in the simulations.

Finally, some computational issues had to be resolved, regarding backflow at the outlet. For this reason, some modifications were made to the functions regarding the thermal profiles: the zone of steep temperature decline after z = 0.6 m was removed, being instead replaced by a flat temperature profile set equal to the temperature measure on the wall at 0.6 m. This did not cause any issues with the simulation results, since these modifications concerned only the last few centimeters of the length of the reactor, the last 10 cm to be exact, a region in which no samples were placed. As such, this change, even though it had small effect on the velocity, temperature, or species distribution fields in the last 10 cm of the reactor, it did not impact the first 50 cm the reactor, in which the samples were placed and studied. As such, the flat temperature profile was able to effectively treat the backflow problem.

The actual code that was used to implement these temperature profiles into the simulations can be found in the appendix.

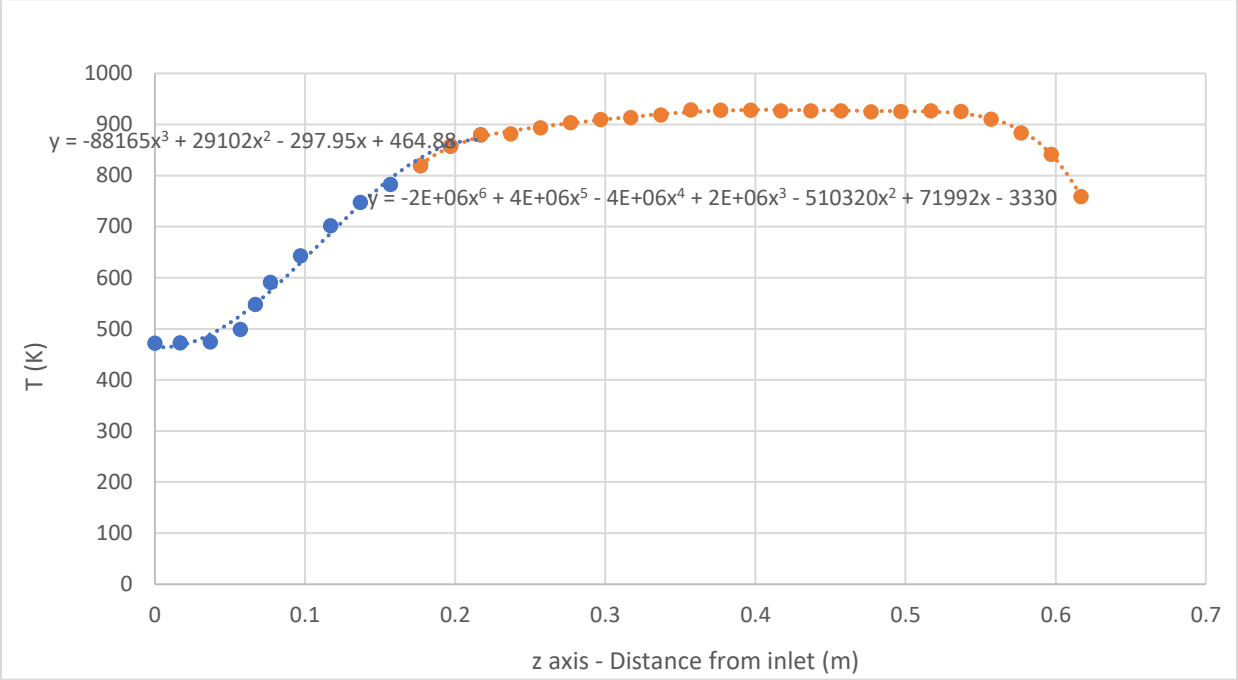

Figure 11. Tubular reactor thermal profile at a set point T=650°C. Experimental measurements are represented by solid circles. Dotted lines show the two interpolated polynomial equations applied in the UDF code.

The temperature profile was implemented using two polynomial equations:

$$p1 = -88165z^3 + 29102z^2 - 297.95z + 464.88 \ (2)$$
$$p2 = -1893242z^6 + 4278394z^5 - 3952366z^4 + 1909960z^3 - 510320z^2 + 71992z - 3330 \ (3)$$

After combining the two polynomial equations at their intersection, we obtain the following temperature function for the thermal profile at the set point T=650°C:

$$T_{650\circ C}(z) = \begin{Bmatrix} p1, & z < 0.20914 \\ p2, & z \geq 0.20914 \end{Bmatrix}, z \ in \ meters$$

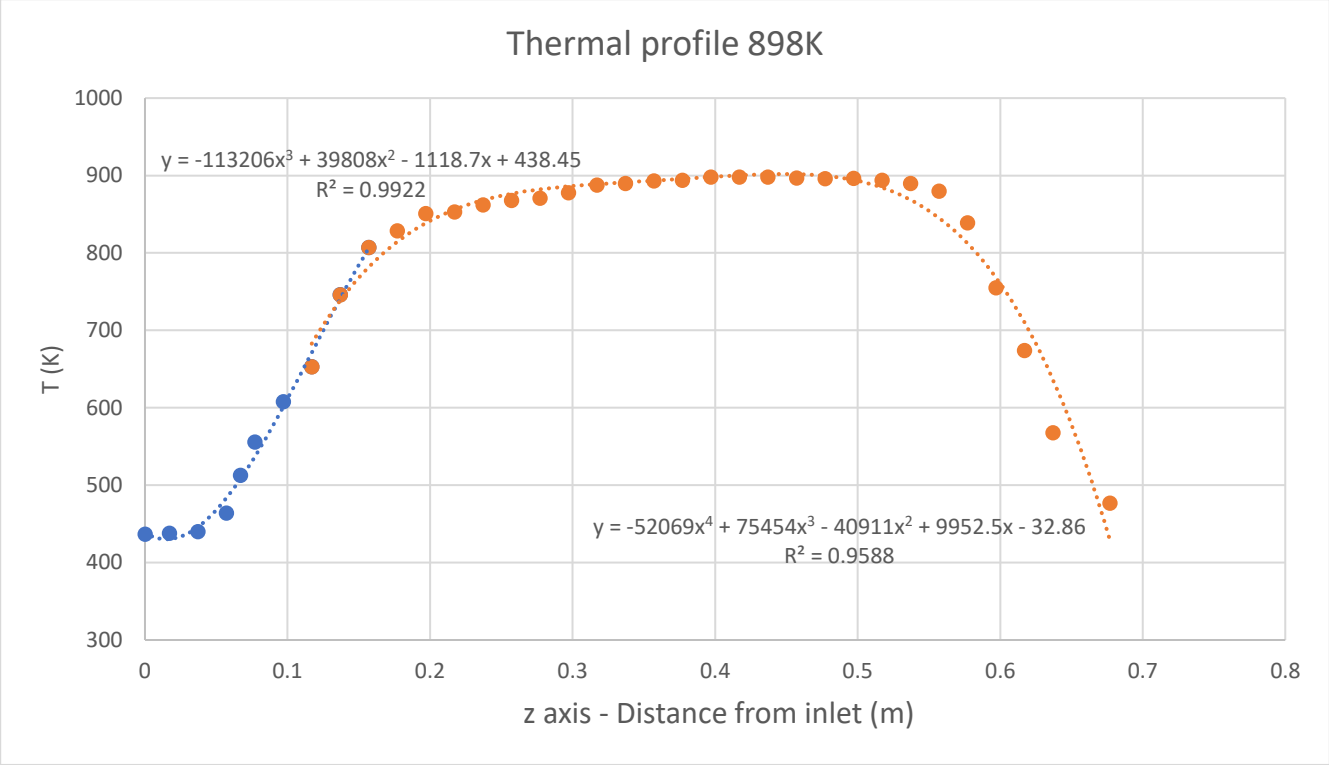

Figure 12. Tubular reactor thermal profile at a set point T=625°C. Experimental measurements are represented by solid circles. Dotted lines show the two interpolated polynomial equations applied in the UDF code.

The temperature profile was implemented again using two polynomial equations:

$$p1 = -113206z^3 + 39808z^2 - 1118.7z + 438.45 \ (4)$$
$$p2 = -52069z^4 + 75454z^3 - 40911z^2 + 9952.5z - 32.86 \ (5)$$

After combining the two polynomial equations at their intersection, we obtain the following temperature function for the thermal profile at the set point T=625°C:

$$T_{625°C}(z) = \begin{Bmatrix} p1, & z < 0.134 \\ p2, & z \geq 0.134 \end{Bmatrix}, z \ in \ meters$$

4.1.2 Solid phase analysis results

The simulations were fitted and modelled on the ellipsometric results which are presented in Table 3.

Table 3. Ellipsometry results regarding the maximum deposition rate and maximum nitrogen content observed across the various experiments.

Experiment Code	T (°C)	Deposition rate nm/min	at.%N
TD3	650	0.54	7
TD4	650	0.9	2
TD5	650	0.2	20
TD6	650	0.6	9
TD7	650	0.65	14
TD8	650	0.54	7
TD9	650	0.24	40
TD11	650	0.44	39
TD12	650	0.83	8
TD14	625	0.39	10

The values taken for the deposition rates as well as for the atomic percentage of nitrogen are the maximum values observed. For the nitrogen content, the maximum value was always encountered on the last sample, sample 18. The position of the maximum deposition rate varied across experiments, and depending on the specific deposition conditions used, it was usually found between the 11th and 14th samples.

We should also mention that the experimental result analysis includes a significant error. The repeatability error is at 7 % while the ellipsometric model has an error of 10 %. In total this adds up to an error of 12.2 %.

$$Total\ error = \sqrt{error_{model}^2 + error_{repeatability}^2} \quad (6)$$

4.1.3 Gas phase analysis results

The gas phase analysis gave two series of results, one by the ESR analysis and one through the GC-MS and NMR.

With the help of ESR, we were able to identify the following species:

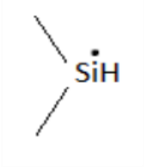

INT(Si)˙

This species was one of the two building blocks implemented in the kinetic model, but it will be discussed more in later stages of this report.

During the time at which this research was being done, the gas phase analysis by GC-MS and NMR could not give quantitative results for the majority of the identified species. Obtaining quantitative results for all by products is a time and resource consuming procedure, since a calibration curve needs to be made for each by-product using the respective standards. Such a calibration curve was made only for the precursor molecule TDMSA. The analysis of the gas phase for all other by-products could thus only provide qualitative information on their presence or absence in each experiment. These species, as provided by the engineer L. Decosterd working on this analysis, can be categorized into six groups. Silylamines, silane, silanols, siloxanes, methoxysilane and water. The actual species can be shown in Figure 13.

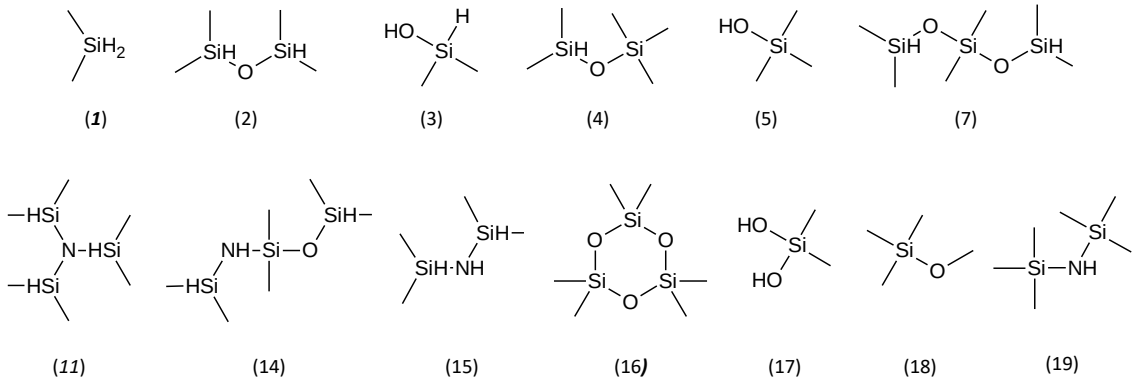

Figure 13. Overview of detected gas-phase by-products by GC-MS.

- Silane : dimethylsilane (***1***)
- Siloxanes : 1,1,3,3-tetramethyldisiloxane (***2***), pentamethyldisiloxane(***4***), 1,1,3,3,5,5-hexamethyltrisiloxane (***7***),hexamethylcyclotrisiloxane (***16***)
- Silanols : dimethylsilanol (***3***), trimethylsilanol (***5***), dimethylsilanediol (***17***)
- Silanamines derivatives : TDMSA (***11***), N-[1-(dimethylsilyloxy)dimethylsilyl]-1,1-dimethylsilanamine (***14***), 1,1,3,3-tetramethyldisilazane (***15***), hexamethyldisilazane (***19***)
- Alkoxysilane : methoxytrimethylsilane (***18***)
- Water

Having these results made the development of the apparent mechanism and subsequently, of the kinetic model a much easier work than it would have been, since many suppositions on how these species were created could be made. Subsequently through these hypotheses, the reality of the gas phase reactions could begin to unmask.

4.2 Theoretical results

4.2.1 Proposing an apparent chemical mechanism

The mechanism constructed at this point is an apparent mechanism. With the term apparent mechanism, we describe, as we have discussed previously the construction of a kinetic model that can recreate the experimental results without including entirely the complexity of the actual chemical system, in order to avoid part of its complexity.

The core of the suggested mechanism derives from a single proposition, the proposition that our reaction starts by the decomposition of TDMSA into two gaseous radical intermediates, as described by the volumetric reaction V1. That means that oxygen does not take part in the core reaction of our system. This position was first suggested, since in none of the gas phase by-products detected contained a N-O bond. This was later confirmed by an experiment using TDMSA (TD9) in absence of O_2 at 650°C and observing the formation of silicon carbonitride material, meaning that TDMSA, at the right temperature is able to deposit on its own. Additionally, later decomposition studies of TDMSA at various temperatures, showed a clear decomposition behavior that depended only on the temperature. Moreover, after the creation of a TDMSA GC-MS calibration curve, the amount of TDMSA exiting the reactor was able to be quantified. Results showed that regardless of the amount of oxygen added in the starting gas phase composition, a similar amount of TDMSA exited the reactor. That led us to conclude that the addition of O_2 does not impact TDMSA composition, and as such, that TDMSA decomposes on its own, aided only by the temperature. Finally, one of the two radicals formed (INT(Si)) was able to be identified by the gas phase analysis, validating this proposition even further.

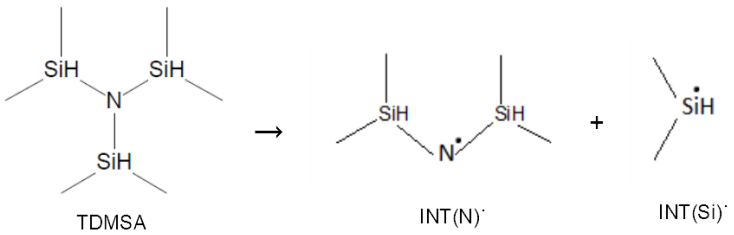

Figure 14. Volumetric reaction V1 indication the decomposition of TDMSA as V1:TDMSA→INT(Si)+INT(N).

Following to the decomposition of the precursor TDMSA, we assumed that two radical intermediates are produced named accordingly INT(N) and INT(Si), which are the reactants for the solid phase reactions and the building blocks for all the gas phase byproducts. It is certain that multiple reactions producing the $SiO_x N_y$ film exist in the studied chemistry. For the purpose of the simulating them in a simplified manner, the two following apparent surface reactions were supposed:

$$\mathbf{S1}\text{: } \mathbf{I}\mathrm{NT(Si)} + \mathrm{O_2} \rightarrow \mathbf{SiO_2}$$

$$\mathbf{S2}\text{: } 4\mathbf{I}\mathrm{NT(N)} \rightarrow \mathbf{Si}3\mathrm{N_4}$$

The total of these three reactions, namely V1, S1 and S2, represented the decomposition of TDMSA and the film formation through two basic deposition reactions. These reactions are the core reactions of the proposed mechanism and are thus the first ones implemented into the simulations. Any additional reactions were added to represent the by-products observed in the gas phase and as a way of further tuning the results of the simulation. The rest of these reactions proposed that produce the by-products are categorized and shown below.

Siloxane reaction path:

1. $2INT(SI)^{\cdot} + O_2 \rightarrow$ 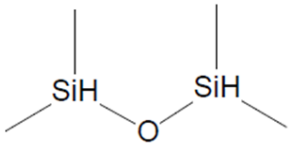 $+O^{\cdot}$

2. 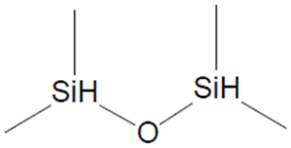 $+INT(SI)^{\cdot} + O^{\cdot} \rightarrow$ 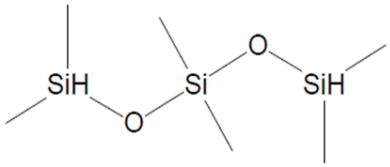 $+H^{\cdot}$

3. 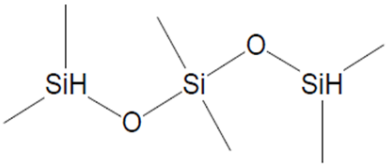 $+O_2 \rightarrow$ 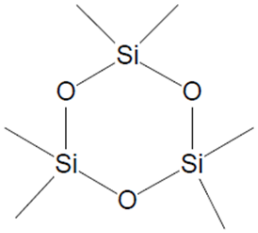 $+H_2O$

Silanol reaction path:

4. 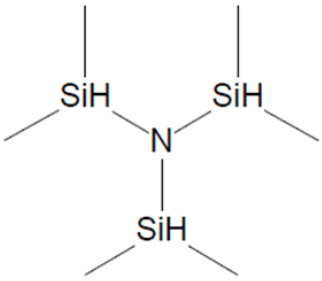 $+H_2O \rightarrow$ 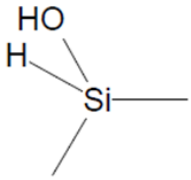 $+$ 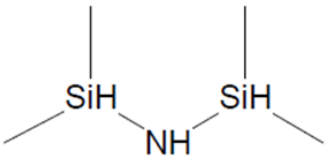

5. 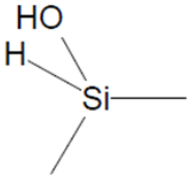 $+2CH_3 \rightarrow$ 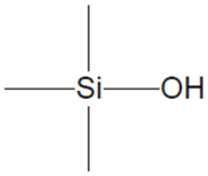 $+CH_4$

Methoxysilane formation:

6. 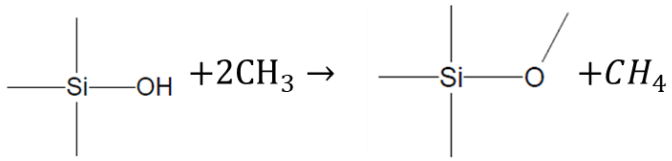

Even though the apparent mechanism can justify the existence of all the by-products, only a few of these reactions were used in the simulations, due to lack of gas phase quantitative results and in order to avoid unnecessary complexity of the system. However, a more complete model would require the addition of some of the chemical reactions presented above.

4.2.2 Strategy of kinetic model development

First, due to the health situation, only the results of one experiment from TDMSA/O_2, TD7, were available at the beginning of the research related to this thesis, and as a result we were obliged to build our model with this very restricted amount of experimental data. The classical procedure to develop such apparent kinetic models of CVD processes is to use the results of at least 4 or 5 different experiments, with different inlet gas composition or deposition temperatures.[5][8] Because of that, we were aware that our first model would be imprecise, and would need to be completed and enriched as soon as more experimental results would be available, which unfortunately occurred at the end of the period of this thesis.

The strategy behind the simulations follows the idea of starting form a basic system and slowly enriching it. For these reasons, our system starts with only V1, which is the decomposition reaction of TDMSA, after which the first solid phase reactions S1, S2 are introduced. Once we have a system that gives us results near to the experimental ones, we start adding more reactions to better fit the experiments and at the same time simulate the production of the by-products. The introduction of these reactions is done through various calculations to extract some initial kinetic parameters and are then manually refined in order to fit the deposition curves given by ellipsometry. It is reminded that ellipsometry follows the two-phase model of SiO_2/Si_3N_4 , and as such, does not represent the presence of carbon and hydrogen in the produced films. In this constant feedback between simulations and ellipsometry the kinetic model takes its form.

4.2.3 Methodology of the calculations

As described before the way the reactions and their kinetic parameters are implemented into FLUENT is through the Arrhenius type expression (Equation 1).

The parameters that we intend to calculate are the pre-exponential factor A_0 , the activation energy E_a, after the implementation of which, FLUENT can give results on the various species concentration profiles, and the calculated deposition rates on each sample. These calculated kinetic parameters are the initial values tested on the simulations and provide us with a good starting point.

4.2.3.1 Partial order exponents

Another important calculation extracted from the experiments is the partial order exponents of the surface kinetic laws, which physically represent the impact of the change in concentration of a reacting species to the reaction rate of the reaction it is participating in.
For estimating them, a series of calculations had to be made. At first, since there are two surface reactions S1 and S2, producing the two solid materials, namely SiO_2 and Si_3N_4, the experimental thickness results had to be divided into 2 via the volumetric fractions taken by ellipsometry. This way the calculations could be made directly for S1 and S2.

$$\mathbf{S1}:\ \mathrm{INT(Si)} + \mathrm{O_2} \rightarrow \mathrm{SiO_2} \qquad \mathrm{k_{S1}}[INT\_Si]^a * [\mathrm{O_2}]^b \quad (6)$$

$$\mathbf{S2}:\ 4\mathrm{INT(N)} \rightarrow \mathrm{Si_3N_4} \qquad \mathrm{k_{S2}}[\mathrm{INT(N)}]^c \quad (7)$$

The calculations for c of S2 were made directly by plotting the equation (8) described below.

$$lnReaction\_Rate = c * \ln([N_{INT}]) + lnk \ (8)$$

The assessment of the a and b exponents of equation (9), was done by comparing experiments for which only the concentration of one of the reacting species, meaning either O_2 or INT_Si, changed. Through this, the impact of the change in concentration of each reactant could be assessed, separately from each other. The experiments that were coupled for these calculations were TD7 and TD12, to calculate the *b* partial order exponent, and TD7 with TD11 to calculate the *a* partial order exponent. An important assumption was made at this point for INT_Si. The assumption is that the relative concentration of TDMSA between the 2 experiments is the same as the relative concentration of INT_Si between them. This way the exponents can be calculated through the following equation:

$$\frac{R_1}{R_2} = \frac{k_{s1}}{k_{s1}} * \frac{[INT_{Si}]_1^a}{[INT_{Si}]_2^a} * \frac{[O_2]_1^b}{[O_2]_2^b} \ (9)$$

At the same time, the calculation for the partial order exponents was done sample by sample obtaining a series of values across the whole length of the reactor. A selection of which values to be taken as an average had to be made. In general, to select these values first we looked at the experimental results of ellipsometry and made a hypothesis on where each solid phase reaction was more probable to be taking place, with the least influence from other reactions. This means that the calculated partial order exponent values that were chosen, would also be less impacted and altered by other reactions potentially taking place in that region of the reactor. At the same time, the selection of these values was also influenced by whether the values selected where giving a desirable shape of a simulated deposition curve. In the end, the chosen values for the partial order exponents were the following:

Table 4. Calculated partial order exponents for the two solid phase reactions, where a is the partial order exponent for the Si_INT, b for O_2, and c for the N_INT.

a	b	c
1.76	0.43	1.2

The partial order exponents though helpful, should be taken with a grain of salt since multiple assumptions were made in order to calculate them. Another source of error in their calculation would be the volumetric fractions taken by ellipsometry since carbon is after all not being taken into consideration for this two-phase model. These results in significant error of the film chemical composition. Another important thing to mention is that the mechanism developed is an apparent mechanism and consists of only a few reactions. Realistically, the reactions happening inside the reactor are many more in number and in complexity. The partial order exponents are calculated for the 2 global solid phase reactions, S1 and S2, and they ignore the existence of other solid phase reactions that also consume the respective intermediates to produce SiO_2 or Si_3N_4.

4.2.3.2 Calculation of the kinetic parameters of the surface reactions

To calculate the kinetic parameters, and more specifically the activation energy E_a and pre-exponential factor A_o of the surface reactions, a different approach had to be taken. The idea is to represent the tubular reactor as a series of slices where the concentration of the gaseous intermediates will be calculated through the mass balance. Except for their length and volume, each of these slices has geometrical characteristics equal to those of the actual reactor. Through this method, we need to assume that each slice has a perfect mix and thus the concentration of any element is homogenous in each slice, since diffusion effects cannot be represented.
The general mass balance is:

$$Inlet - Outlet = \pm Accumulation \pm Consumption$$

Being in a steady state we have:

$$Accumulation = 0\ mol/s$$

The mass balance for INT(N) gets the following form:

$$[INT(N)_{i+1}] = \frac{[INT(N)_i] * Q_i + V1 * Slice\_volume - S2 * Surface}{Q_{i+1}} \quad (10)$$

With the value of the intermediate concentration of the first slice *i* being supplied by running reaction V1 in the simulation environment.

Then the kinetic parameters are calculated through plotting the rate equation.

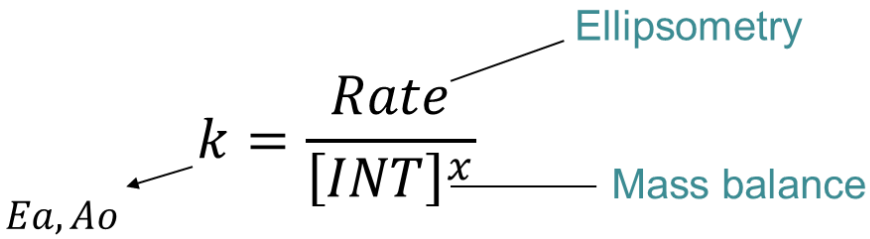

These parameters that are calculated cannot be a perfect calculation that will immediately give us the kinetic model that fits the experiments. They are rather the starting parameters that will give us a good starting point in order to continue with manual optimization.

4.2.3.3 Measurement of the TDMSA conversion rate

There are two important pieces of information that can be extracted to assist in the correct implementation of V1.

First, the analysis of the gas phase has given the following results regarding the TDMSA conversion, with an error range of 11%:

Table 5. Calculated TDMSA conversion across the various experiments.

Experiment	TD4	TD5	TD6	TD7	TD8	TD9	TD11	TD12
Conversion (%)	82	81	81	81	80	81	86	82

Therefore, there has been a conversion calculated of 81% and that will help fit V1 closer to reality.
An interesting point to note at this point is that all experiments show more or less the same conversion even though some contain NH_3 and all have different O_2 flow rates. This is an extra verification that the mechanism begins with the thermal decomposition of TDMSA, and without the aid of any extra species.

In order to calculate the kinetic parameters of V1, another series of experiments took place with the starting conditions of TD9 (2 sccm TDMSA, absence of O_2) but at various temperatures. Specifically, 580, 625, 650 and 700°C. The reason behind these experiments is to assist in calculating the activation energy E_a for V1 through the TDMSA conversion at different temperatures. The results were the following:

Table 6. Calculated TDMSA conversion after its decomposition at different temperatures.

Experiment	580°C	625°C	650°C
Conversion (%)	10	40	81

As expected at lower temperatures the TDMSA conversion decreases significantly.

Assuming the reactor as a plug flow reactor (PFR) we calculate from the mass balance:

$$Q * C_x - Q * C(x + dx) = V * \frac{dC}{dt} \quad (11)$$

$$V = S * dx \quad (12)$$

We are assuming steady-state regime with the conditions at a given location in the PFR being constant. For a first order reaction we have:

$$\frac{dC}{dt} = -kC \quad (13)$$

Combining the equations (9), (10) and (11) and integrating for the length L of the PFR we get:

$$\frac{C_{out}}{C_{in}} = \exp\left(\frac{-k * S * L}{Q}\right) \quad (14)$$

The conversion is expressed as:

$$X = (C_{in} - C_{out})/C_{in} \quad (15)$$

Correlating the conversion through (13) to the reaction rate kinetic constant *k* through (12), we get:

$$X = 1 - \exp\left(\frac{-k * S * L}{Q}\right) \quad (16)$$

Calculating for the above experiments, we find the kinetic parameters:

$$Ea = 250.66\ kJ/mol$$
$$A_0 = 0.18$$

These values are acceptable since, as we have explained before, we are constructing an apparent kinetic model and thus its kinetic parameters need to be able to recreate the experiments, rather than be theoretically correct.

4.2.3.4 TDMSA yield calculation

The final series of calculations that was performed related to the yield of TDMSA, meaning the amount of TDMSA that got converted into SiO_xN_y on the solid phase or that was transformed in to gas-phase by-products that didn't lead to film formation. This calculation, even if we do not need it directly to perform the simulations, can give an insight on how much of our reactant ends up on the solid phase and how much leaves the reactor unreacted or gets converted into gas-phase by-products.

The yield calculation was made for the experiment TD7 and is a correlation between the TDMSA consumption inside the bubbler and the mass gain on all the 18 substrates after the end of the experiment.

The results were as follows:

$$TD7_{TDMSA\ yield} = 0.087\%$$

Seeing this low value for the yield while having a relatively high conversion (81% ± 11% as taken from the GC-MS analysis), it becomes obvious that the biggest part of the TDMSA that enters the reactor, ends up being converted into non film-forming gas-phase by-products. This realization is very important since it correlates well with the high quantity of the identified by-products, for which we only had qualitative results for so far, as well as the significance of enriching the system with many gaseous, apparent reactions to better represent the system in the simulations. More about this issue will be discussed in the perspectives section of this report.

4.3 Simulation results

The simulations were based on experiment TD7 as it was the only one for which enough experimental data were available due to the health situation related to COVID-19.

The total mass flow for the simulation is:

$$MassFlow = 8.38763 * 10^{-5}\ kg/s$$

The mass fractions of the species at the inlet as calculated for experiment TD7 are:

$$TDMSA = 0.0026494$$
$$O_2 = 0.0001697$$
$$N_2 = 0.9971809$$

The simulations begin with the introduction of the first volumetric reaction V1. The simulation uses the calculated kinetic parameters of V1.

	Reaction Stoichiometry	**ReactionRate and Kinetic constants**
Volumetric Reactions $(\mathrm{kmol/m^3 s})$ (V1)	$\mathrm{TDMSA} \rightarrow \mathrm{INT(N)} + \mathrm{INT(Si)}$	$\mathrm{k}_{V1}[\mathrm{TDMSA}]$ $\mathrm{k}_{V1} = 0.18 \times \exp\left(-\frac{250.66}{\mathrm{RT(K)}}\right)$

The code for this simulation is simV900 and the profile of the simulation is presented below.

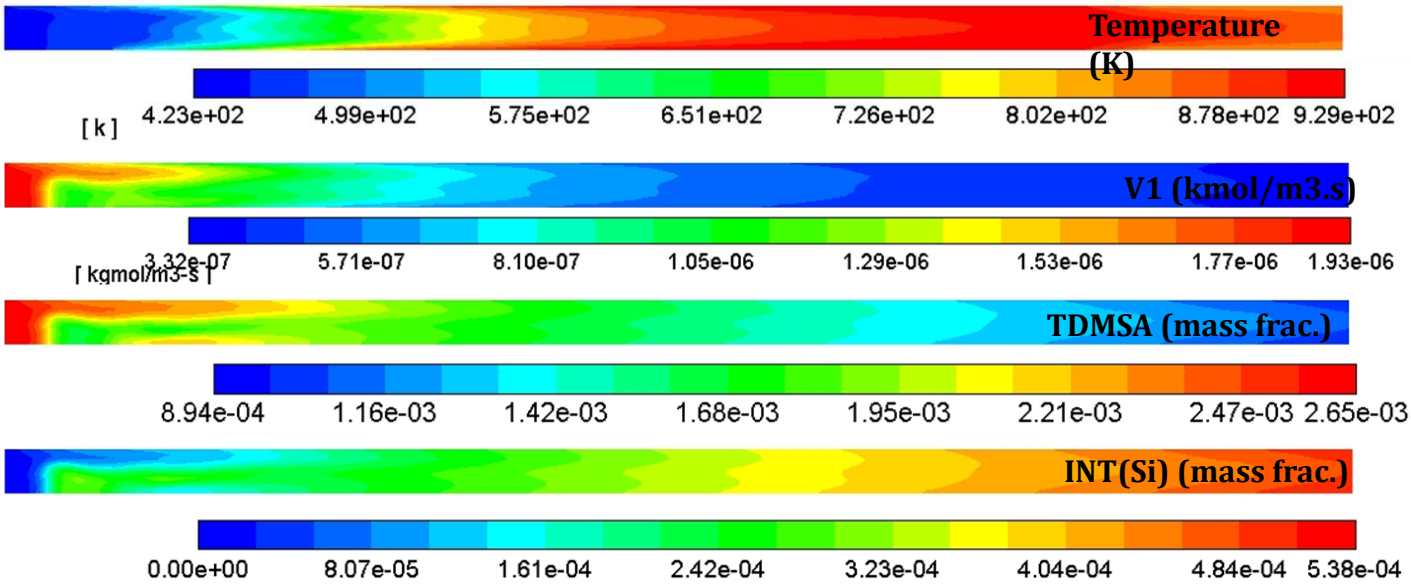

Figure 15. SimV900 profile.

The contour of INT(N) was not presented as it has the same form as the one of INT(Si).

Something that we can observe from this starting simulation is that V1 is very active and takes place mostly at the very first part of the reactor. As a result, the two intermediates produced are present from early on even though the deposition begins only after around 0.18 m of the reactor. This could be an indication it is S1 and S2 that define the temperature that the deposition will occur rather than V1 since V1, the decomposition of TDMSA appears to take place even at low temperatures.

Following the introduction of V1 we introduce the solid phase reactions S1, S2 with the simulation simV901. The kinetic parameters of this simulation were implemented as calculated from the sliced reactor calculation sheet, that has been described in a previous paragraph.

Table 7. SimV901 kinetic parameters.

simV901	Ea (kJ/mol)	A
S1	1.98E+08	9.88E+13
S2	2.12E+08	2.32E+08
a	**b**	**c**
1.76	0.43	1.2

The deposition profiles obtained by simV901 are the following:

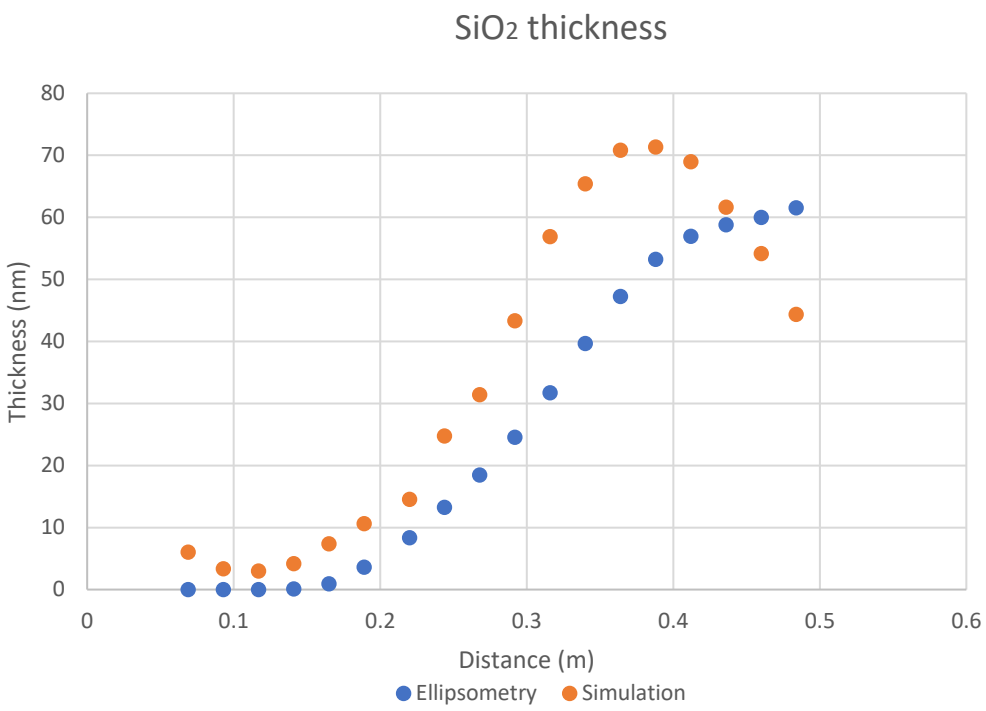

Figure 16. Comparison of the SiO_2 thickness between simulation simV901 and ellipsometry.

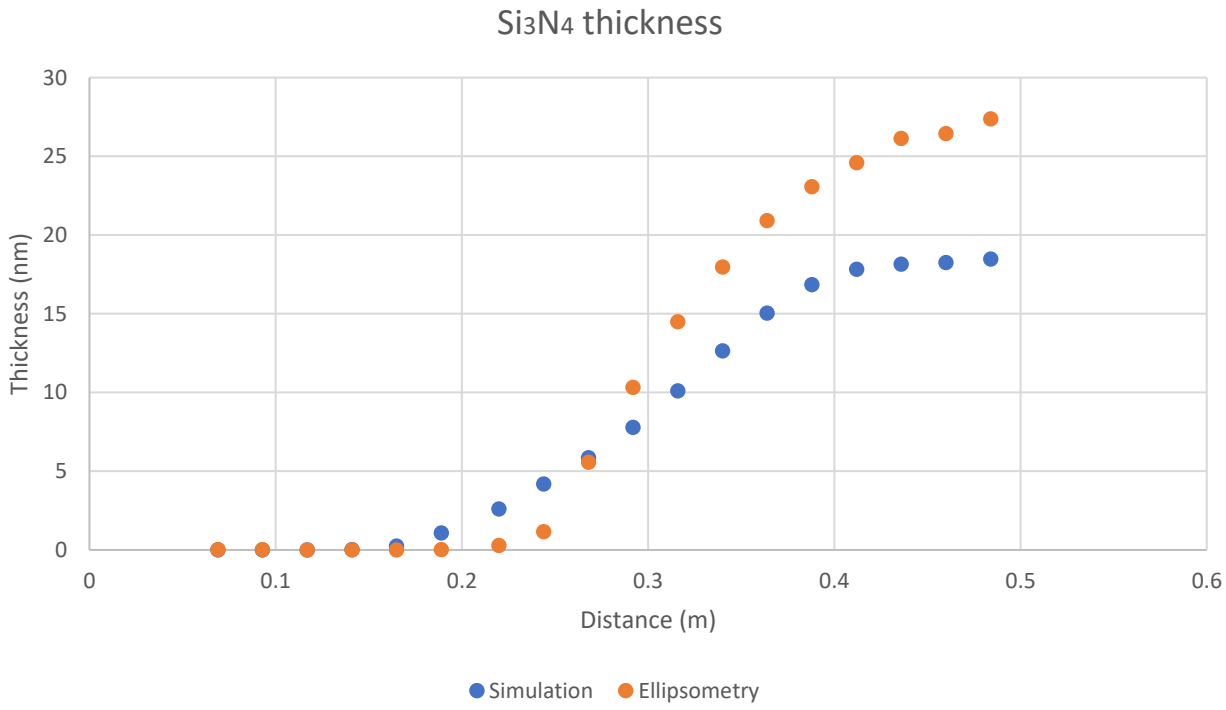

Figure 17. Comparison of the Si_3N_4 thickness between simulation simV901 and ellipsometry.

The kinetic values calculated by the sliced reactor gave a very good starting point for fitting the depositions. These results though, are not satisfactory and thus further manually optimization is required.

SimV902 produced the optimized results that are presented below.

Table 8. SimV902 Kinetic parameters

simV902	Ea (kJ/mol)	A
S1	1.70E+08	5.00E+12
S2	4.00E+08	1.20E+19
a	**b**	**c**
1.76	0.43	1.2

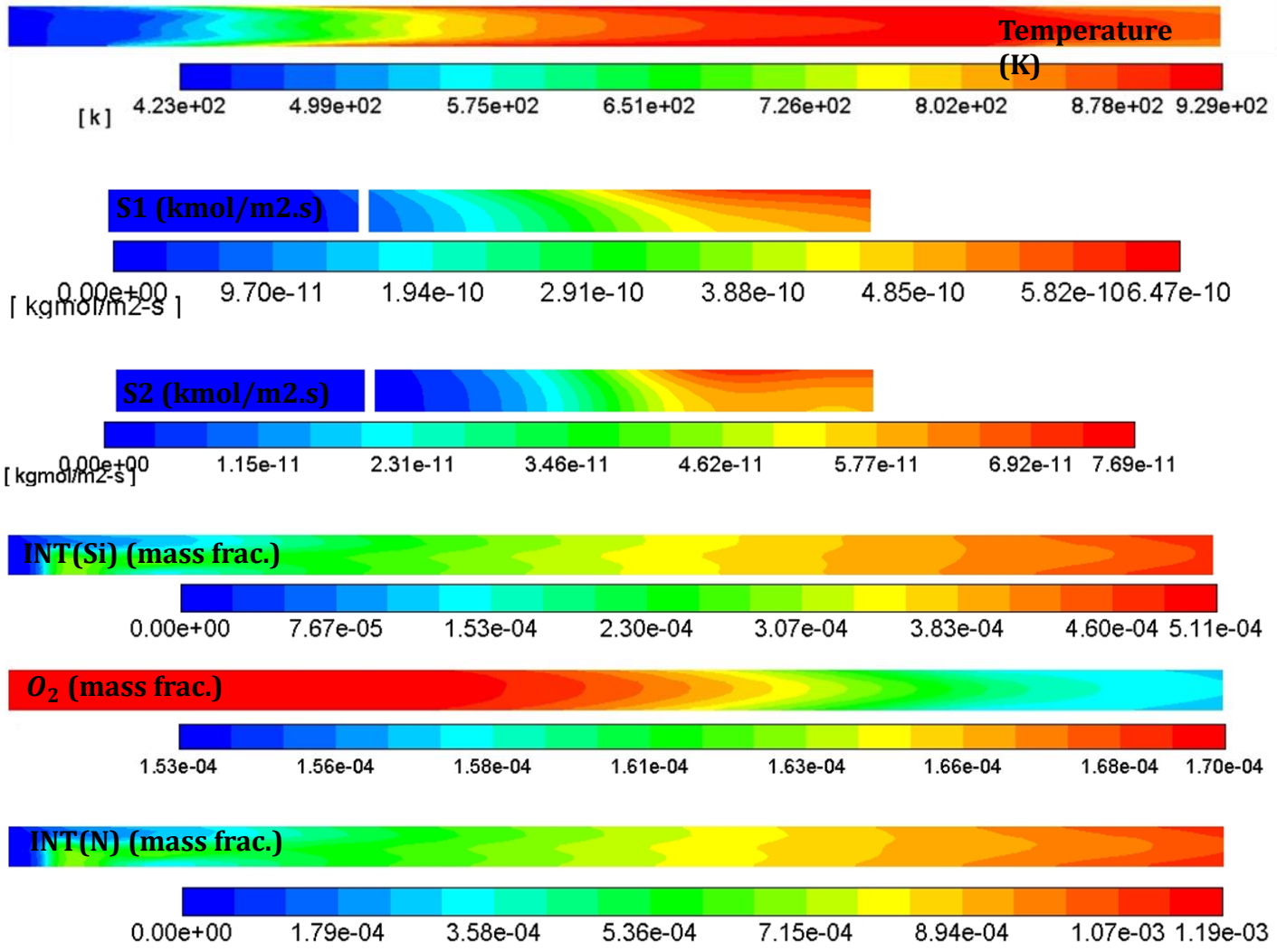

Figure 18. simV902 profile

An interesting observation of these contours is that O_2 is hardly consumed by S1. This is an observation that leads into thinking of adding O_2 consuming reactions in order to regulate better its consumption and have more control over S1 and thus the SiO_2 deposition.

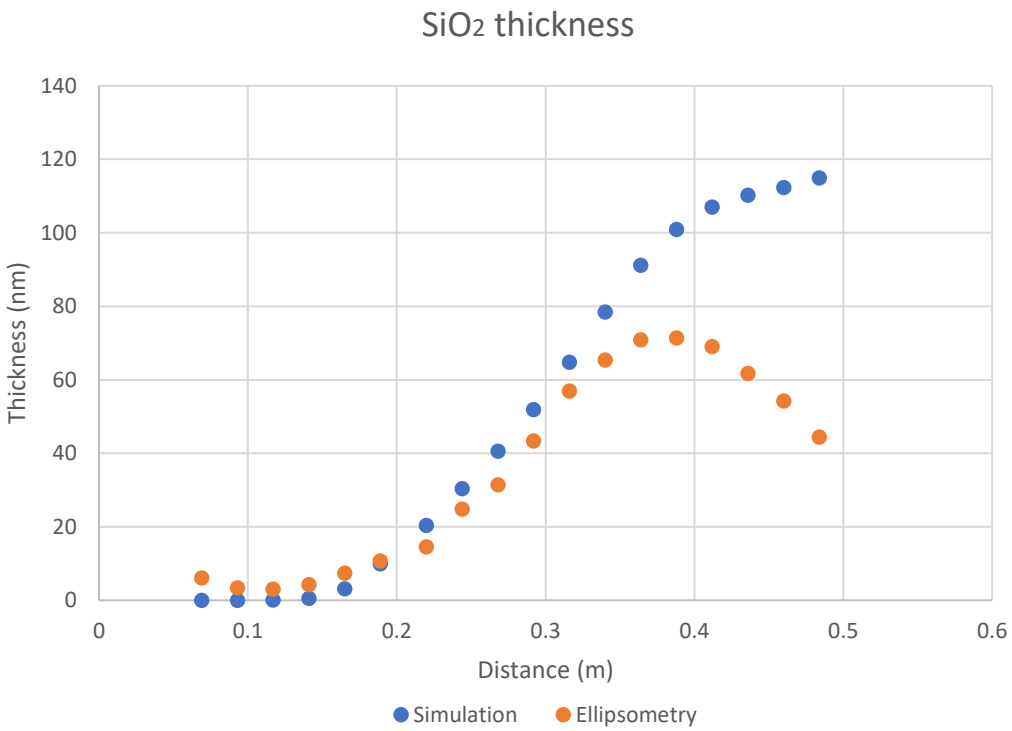

Figure 19. Comparison of the SiO_2 thickness between simulation simV902 and ellipsometry.

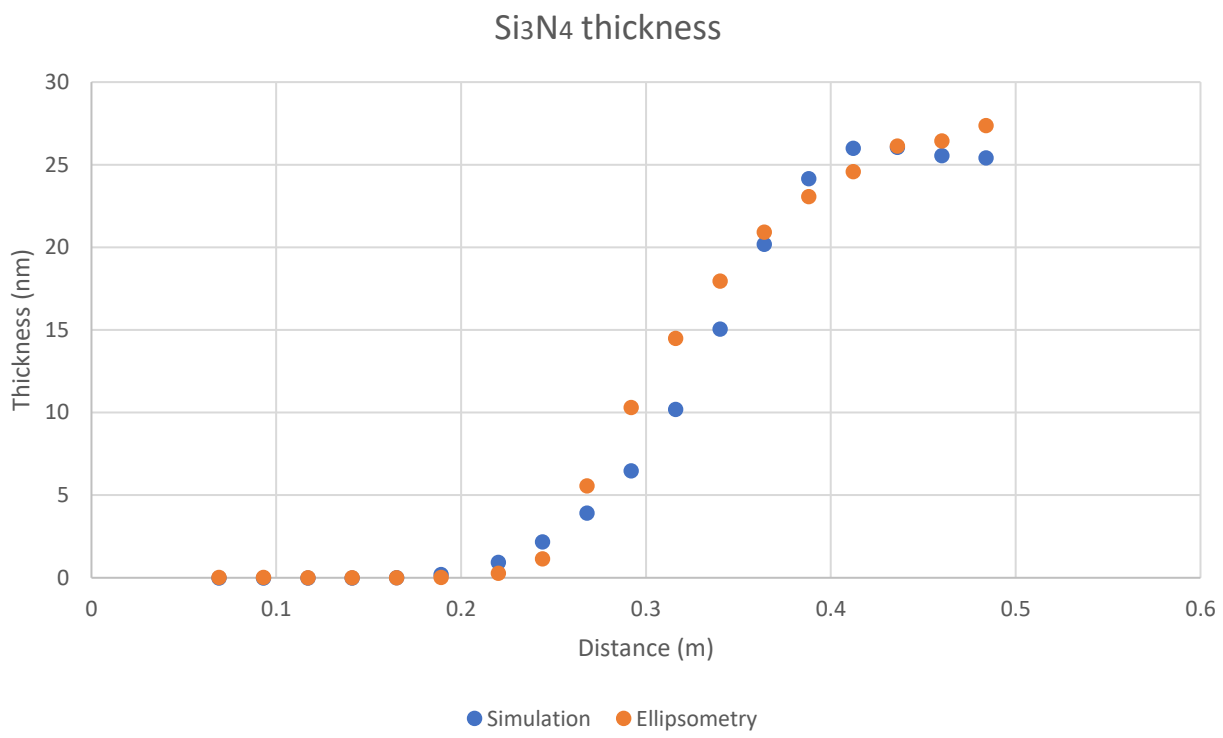

Figure 20. Comparison of the Si_3N_4 thickness between simulation simV902 and ellipsometry.

The results of simV902 show that S2 has been fitted well since the Si_3N_4 deposition of the simulation follows relatively closely the one of ellipsometry even though the simulation appears to have a peak contrary to the results of ellipsometry. At the same time, it shows the need of complexifying the kinetic mechanism of silica since the SiO_2 deposition seems to have a different shape between simulation and ellipsometry. A need for a new volumetric reaction is evident.
This volumetric reaction is V2.

$$\boldsymbol{V2:\quad 3INT(Si)^{\cdot} + 2O_2 \rightarrow Siloxane + H_2O}$$

The reason Siloxane was selected as the by-product in place of another by-product observed by the gas-phase analysis, like a silanol, is based on the fact that we observe multiple species of the siloxane family and the mechanism suggested for the siloxane formation is a direct derivative of a reaction between INT(Si) and O_2, the two species that we want to regulate.

V2 will be a competitive reaction to S1 and in this way more control over the SiO_2 deposition will be obtained. The limiting element of S1 is O_2 as it can be observed by the contours of simV902 (Fig 18). The calculation of the kinetic parameters of V2 will be made through searching for a reaction that consumes enough O_2 to allow S1 to give a deposition as the one of ellipsometry.

First the oxygen concentration that will give the ellipsometry deposition curve on the current model needs to be calculated. This is achieved in the following way:

$$[O_2]^b = \frac{Rate}{[INT(Si)]^a * k} \quad (17)$$

With the rate of the reaction coming from ellipsometry while k being calculated by the kinetic parameters on the current model (simV902).

Considering V1, S1 and INT(Si) known from the current kinetic system we make the mass balance.

$$R_{V2} = \frac{(Q_i * [O_2]_i - Q_{i+1} * [O_2]_{i+1} - R_{S1} * S_{slice})}{V_{slice}} \quad (18)$$

Making the Arrhenius plot we can then find the kinetic parameters of V2.

Calculating the parameters of V2 as described above, recalculating these of S1 and implementing them on FLUENT in simulation simV904, the following results are obtained:

Table 9. SimV904 Kinetic parameters.

simV904	Ea (kJ/mol)	A
S1	1.86E+08	1.81E+13
V2	5.26E+08	2.72E+35

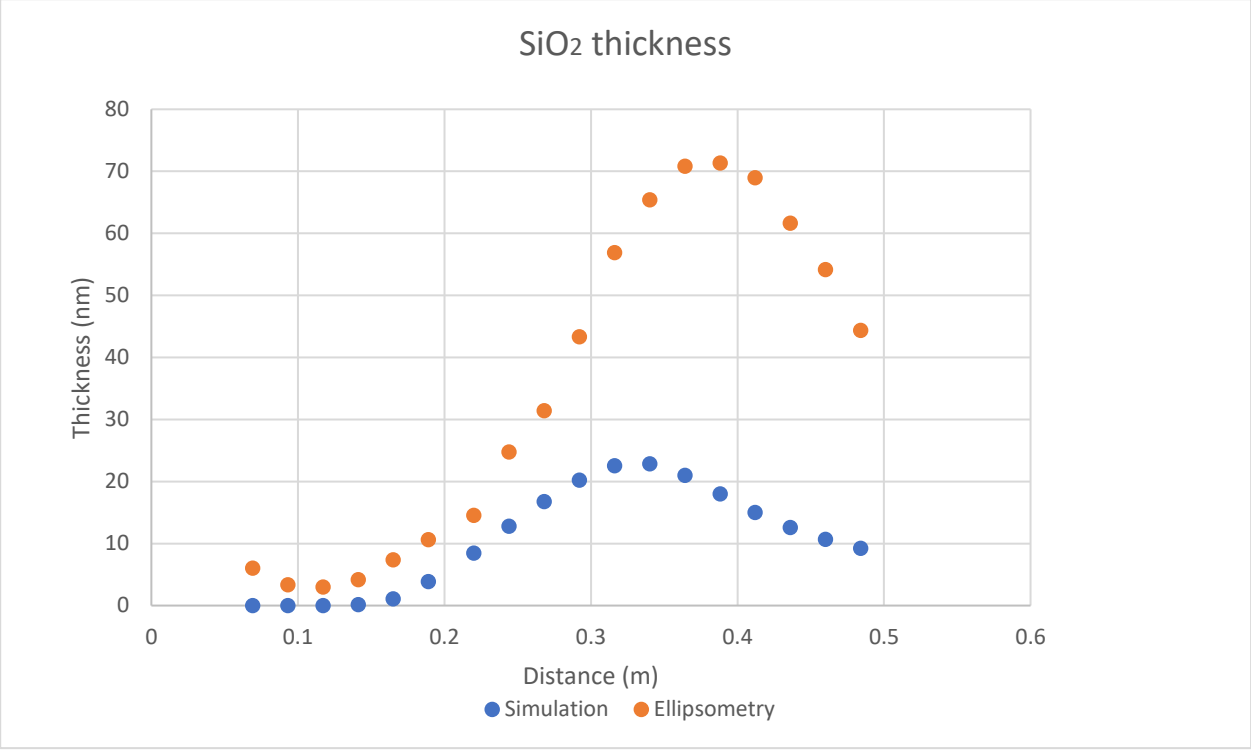

Figure 21. Comparison of the SiO_2 thickness between simulation simV904 and ellipsometry.

The shape of the SiO_2 deposition curve after the introduction of V2 has been improved. However further manual manipulation is required. This manual manipulation will, for the most part be a result of increasing the intensity of S1.
The results of the Si_3N_4 are not shown here as they do not change from simV904 and onwards.

Simulation simV907 is the final simulation for TD7 and its results are presented below.

Table 10. SimV907 Kinetic parameters after manual fitting.

simV907	Ea (kJ/mol)	A
S1	3.00E+08	1.00E+20
V2	5.26E+08	7.00E+34

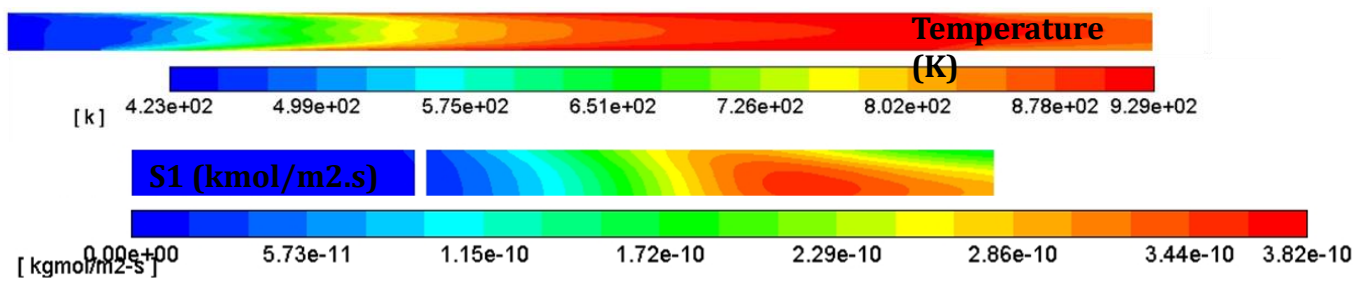

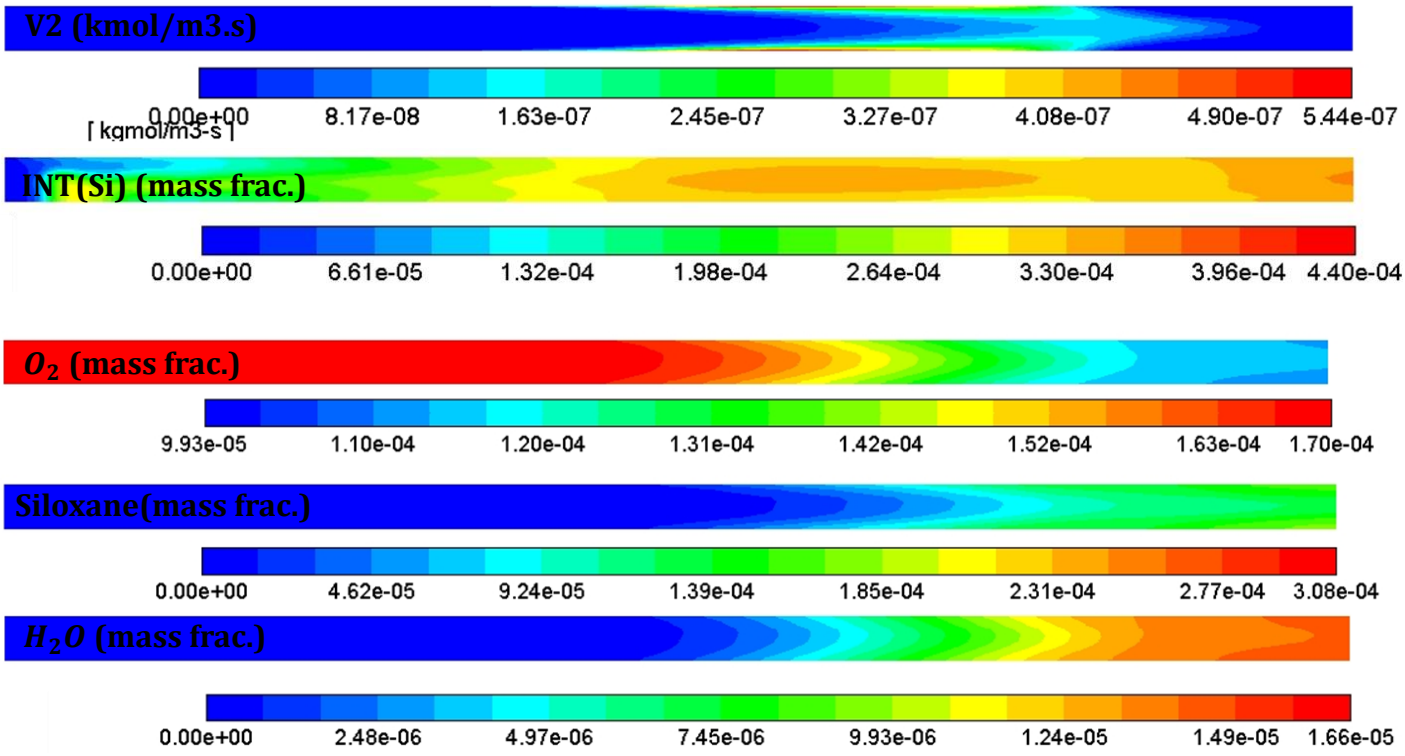

Figure 22. simV907 profile.

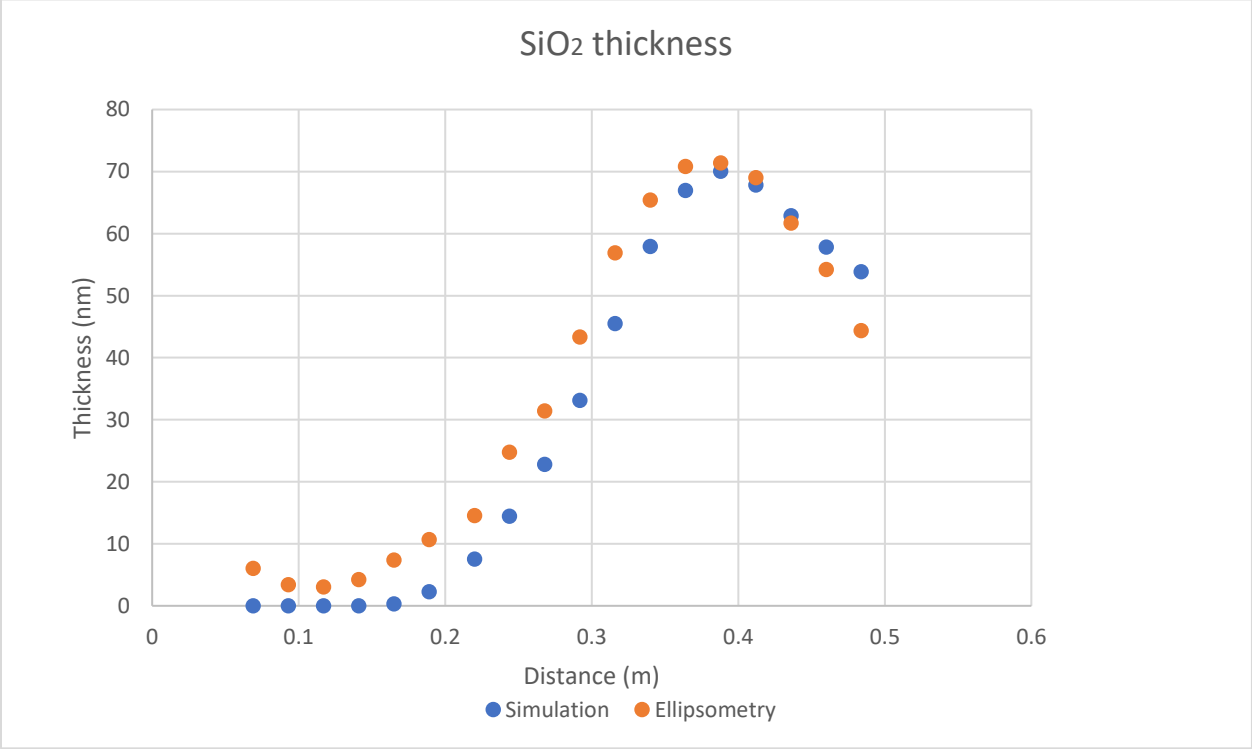

Figure 23. Comparison of the SiO_2 thickness between simulation simV907 and ellipsometry.

Finally, the SiO_2 deposition has been satisfyingly fitted and the kinetic mechanism has been formed. Something can be noticed though is that the SiO_2 deposition starts 2 samples later on the simulations. This will result in an overestimation of the nitrogen at.% at this region, as will be discussed later on.

The profile of the total thickness is as follows:

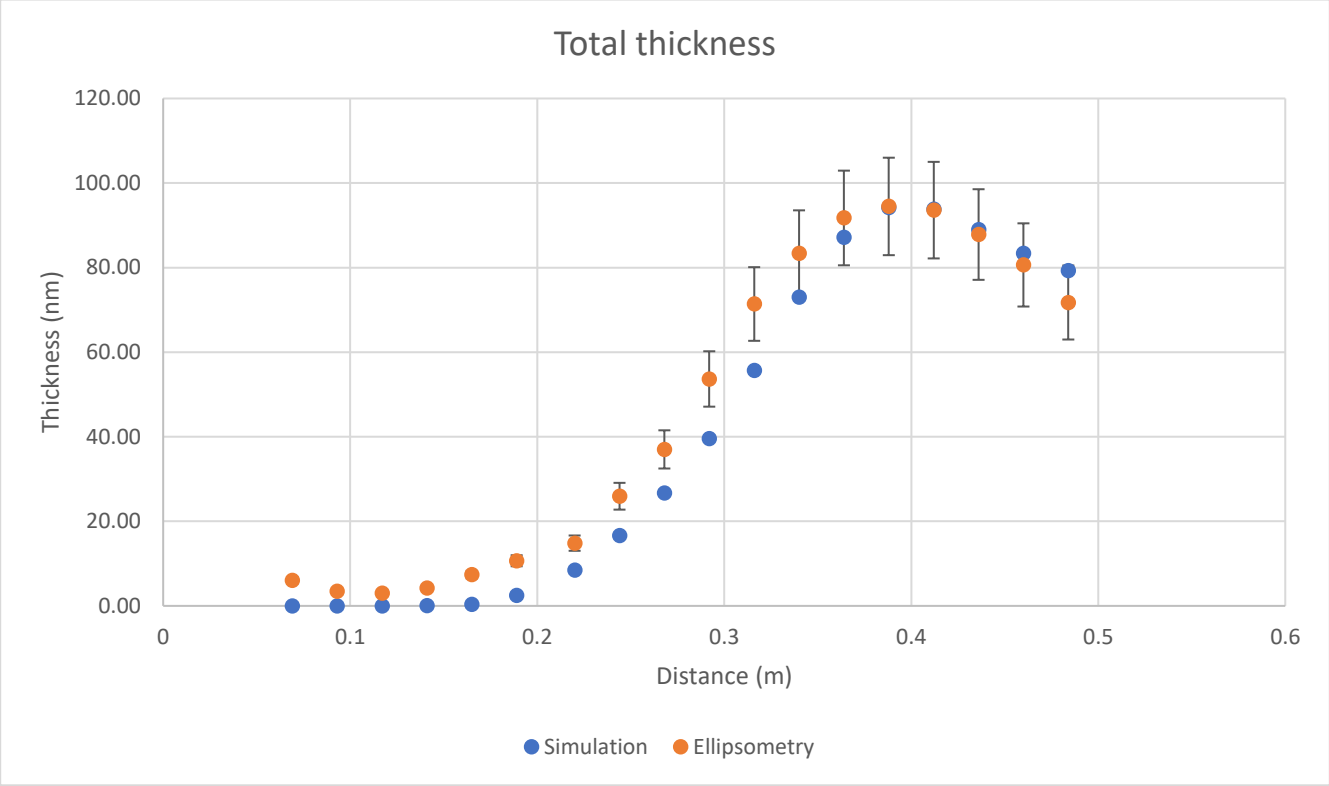

Figure 24. Comparison of the total thickness between simulation simV907 and ellipsometry.

The experimental error bars are added in this graph only since it represents the final result of the fitting attempts on TD7.

Figure 25. Photograph of TD7 deposition on silicon substrates (top). Contour of simulated deposition profile (bottom).

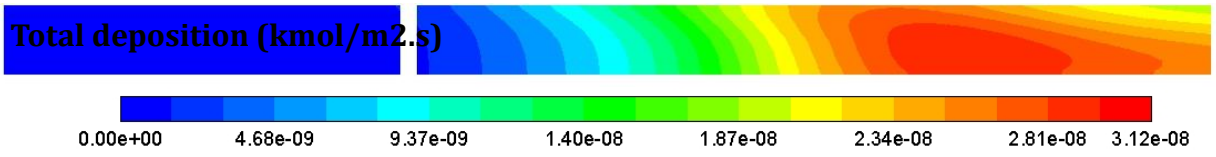

Table 11. Final values of the kinetic parameters used in the developed model.

Kinetic system	Ea (kJ/mol)	A
V1	2.51E+02	1.80E-01
S1	3.00E+08	1.00E+20
S2	4.00E+08	1.20E+19
V2	5.26E+08	7.00E+34
a	**b**	**c**
1.76	0.43	1.2

Table 11 shows the final set of reactions and kinetic parameters. The proposed chemical model with above reaction kinetic were tested on the other experiments of the $TDMSA/O_2$ chemical system in order to check the performance of the developed simulation mechanism.

4.4 Evaluation of the developed model through simulation of the parametric analysis using TD7, TD11, TD12, TD14

In this section the results obtained after applying the developed deposition mechanism with the calculated reaction kinetics to the rest of the experiments are presented.

Table 12. Experimental conditions of the experiments in analysis.

TDMSA = 2sccm	O_2 $(sccm)$	T°C
TD11	0.3	650
TD7	0.6	650
TD12	1.2	650
TD14	0.6	625

4.4.1 Deposition rates

The biggest part of this search through the simulations was given into fitting the deposition rates of each experiments. The results of this effort after applying the kinetic model developed on TD7 on the rest of the experiments are presented in the following sections.

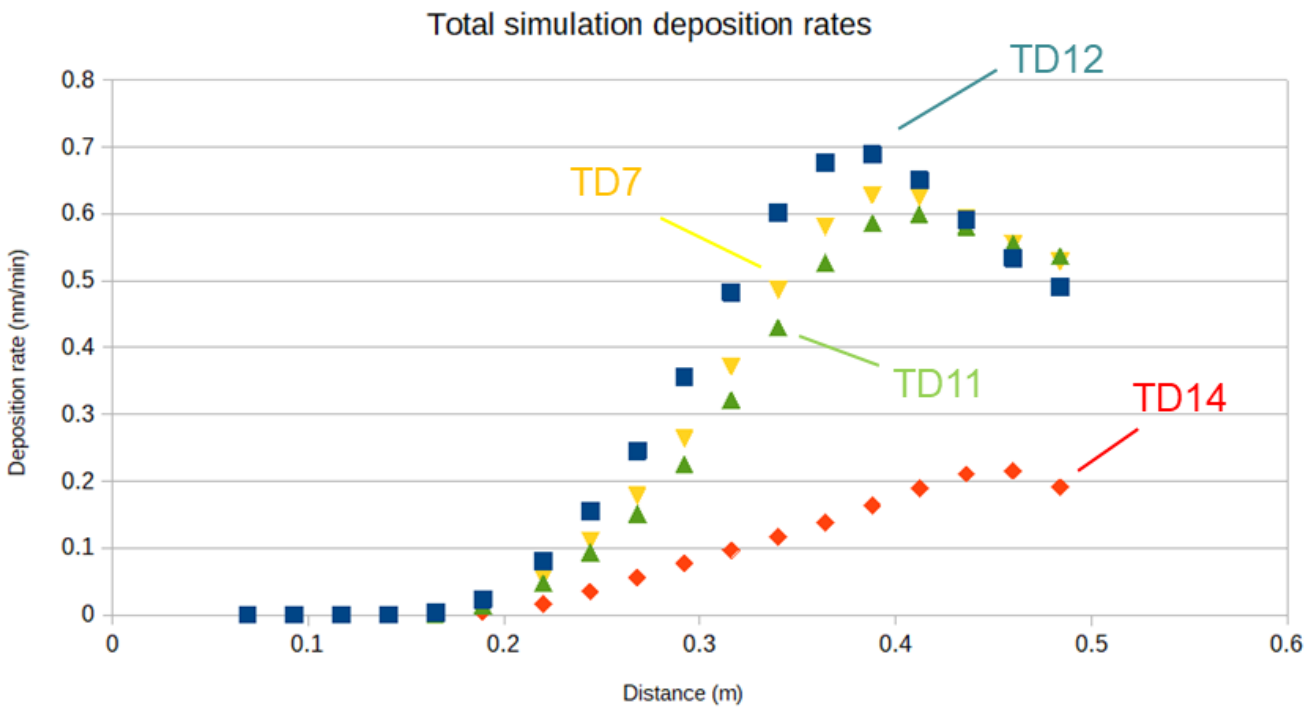

Figure 26. Comparison of the simulated total deposition rates between the 4 experiments in question.

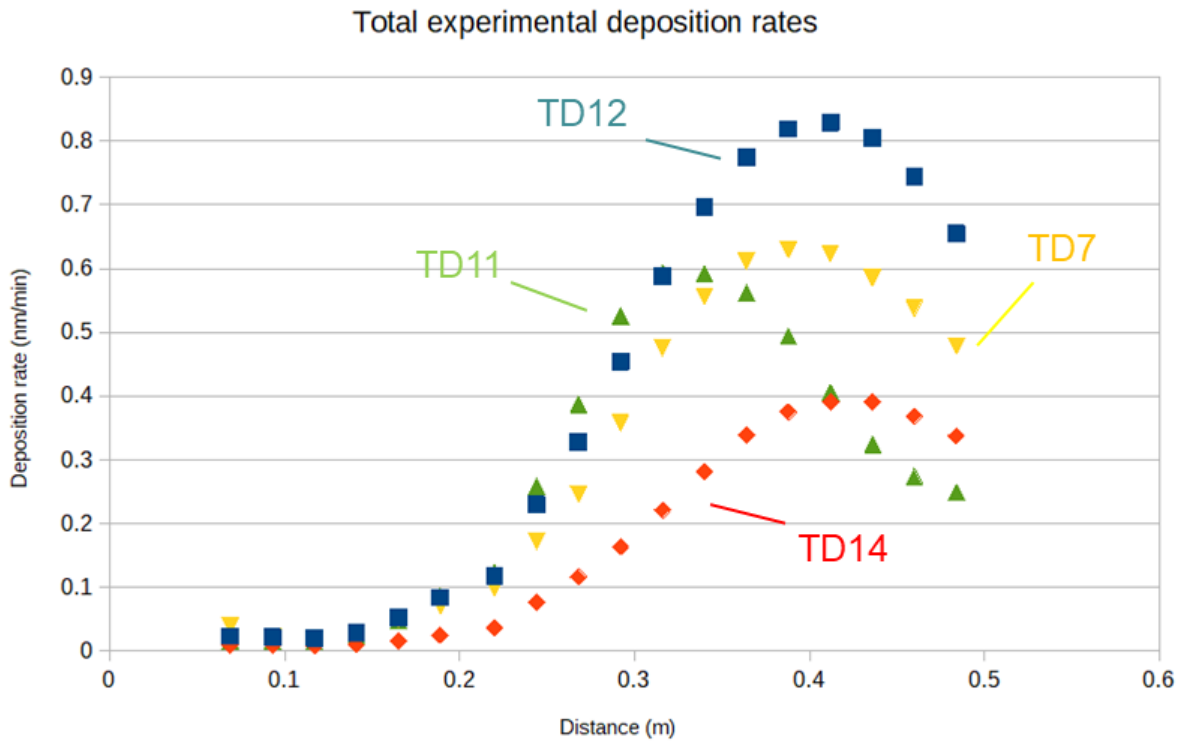

Figure 27. Comparison of the experimental total deposition rates between the 4 experiments in question.

Comparing the behavior of the deposition rates between the simulations and ellipsometry, one can notice a few things. Firstly, moving from low to high O_2 flow rate (TD11→TD7→TD12), a different behavior of the maximum of the deposition rates is observed. In the simulations, the maximum of the deposition rate curves moves to the left with increasing the oxygen flow rate, having the TD12 curve peak as the most left one. In the results of ellipsometry, the opposite phenomenon is observed where higher O_2 flow rate shifts the maximum to the right, having TD11 curve peak as the leftmost one. This is an important observation that mildly undermines the credibility of this first simulation mechanism, as we have feared.
Also, focusing on the experiments TD7 and TD14, which were conducted for the same flow rates but at different temperatures, one can notice that the simulation underestimates the deposition rate, having though a good result for the peak position of TD14.

The experimental and calculated deposition rate results of each experiment separately are presented below.

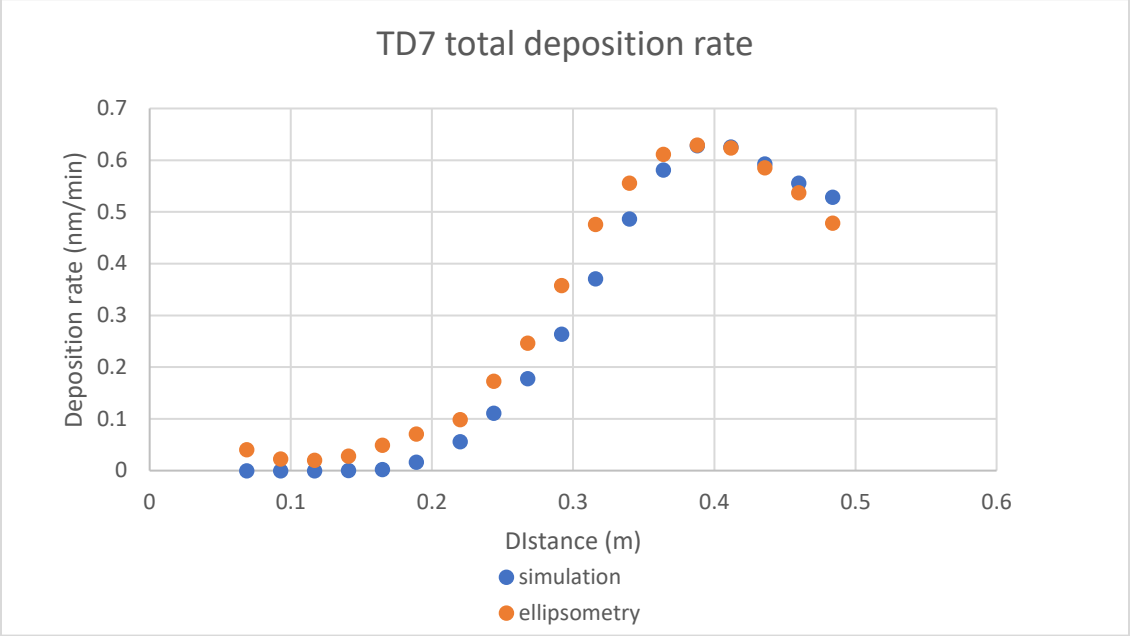

Figure 28. Comparison of the total deposition rate between simulations and ellipsometry for experiment TD7.

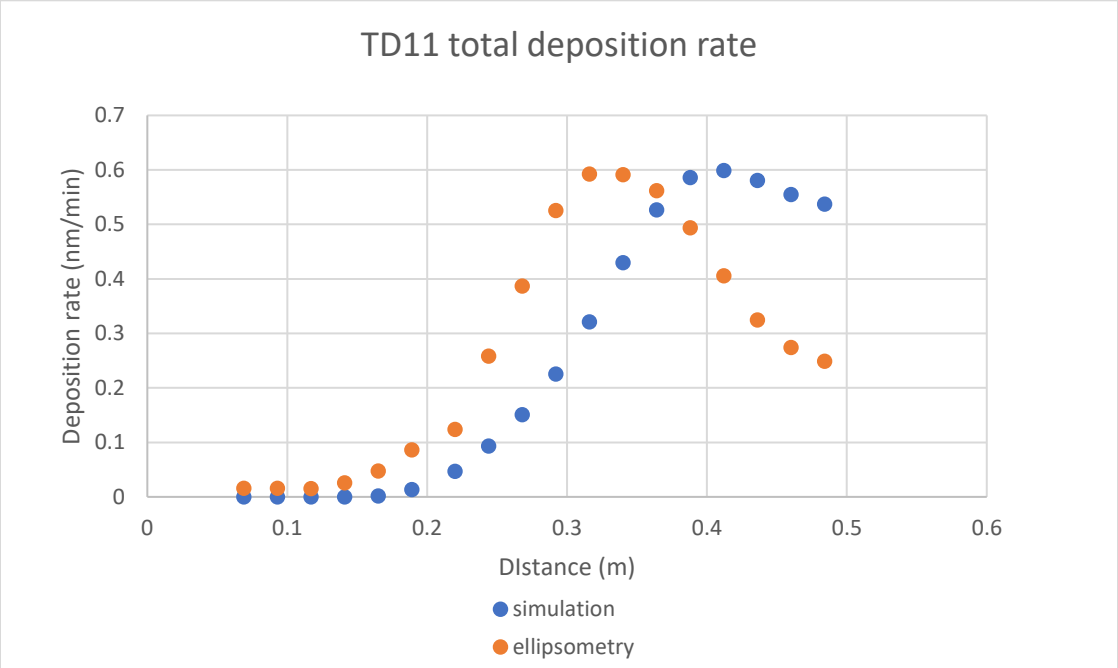

Figure 29. Comparison of the total deposition rate between simulations and ellipsometry for experiment TD11.

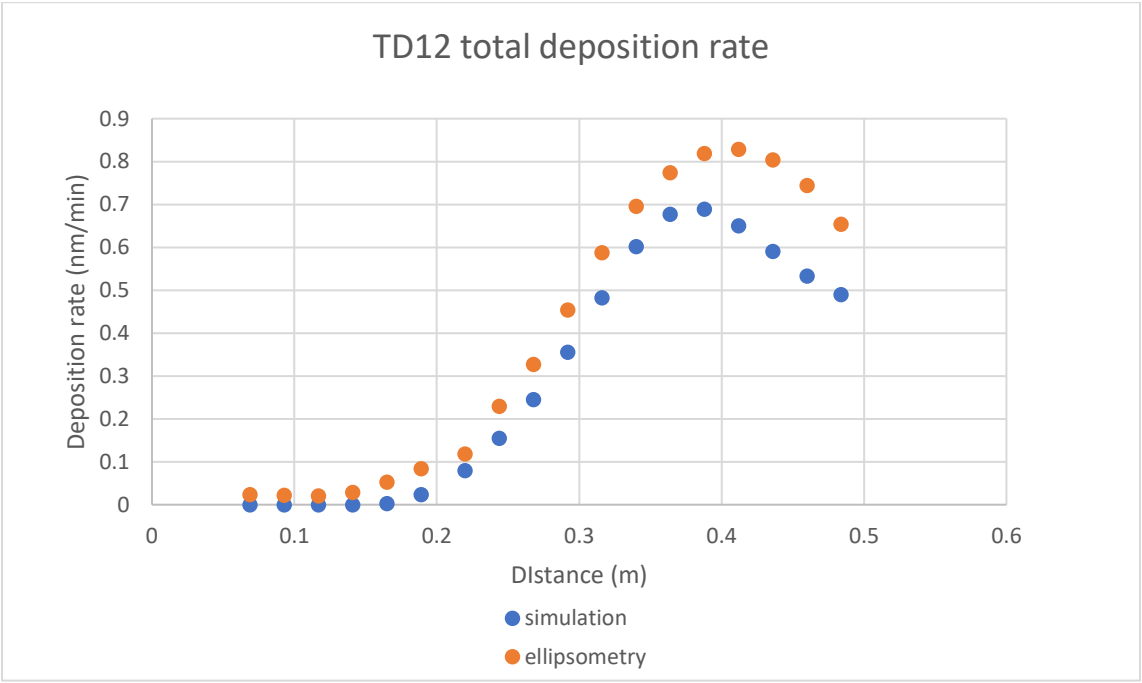

Figure 30. Comparison of the total deposition rate between simulations and ellipsometry for experiment TD12.

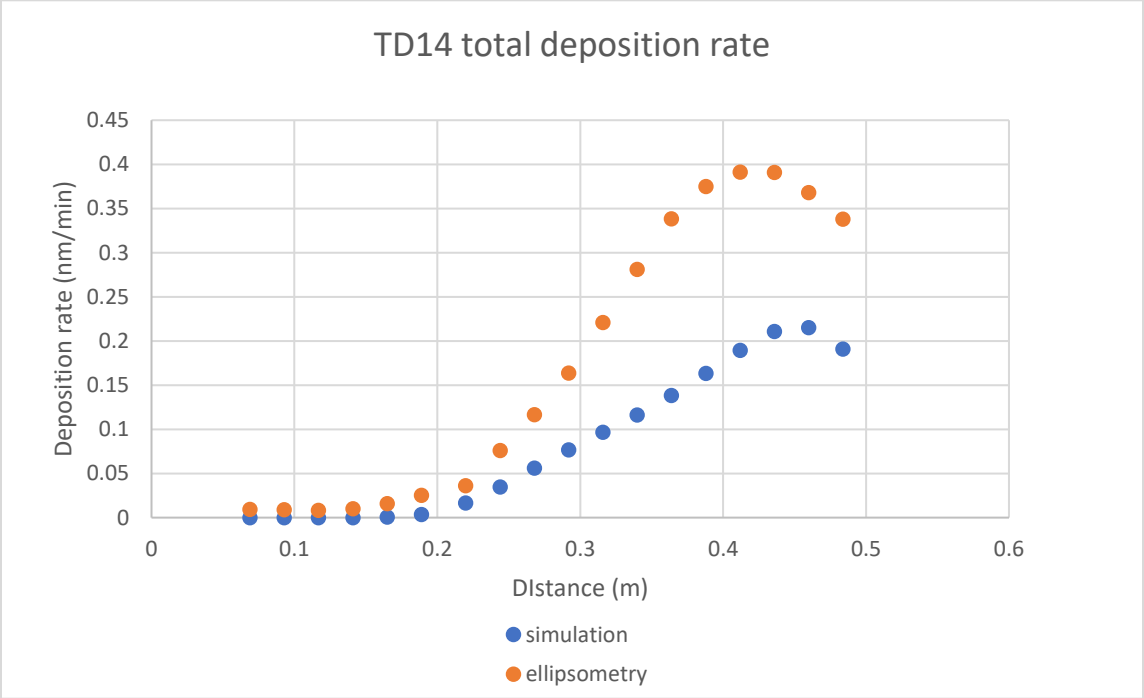

Figure 31. Comparison of the total deposition rate between simulations and ellipsometry for experiment TD14.

4.4.2 Atomic N%

Beyond the deposition rate of the solid phase reactions, the atomic percentage of nitrogen in the film is also of high interest, since it is through the addition of nitrogen that the film gains the desired insulation properties.

First, the comparison between simulation and ellipsometry on the experiment TD7 is presented.

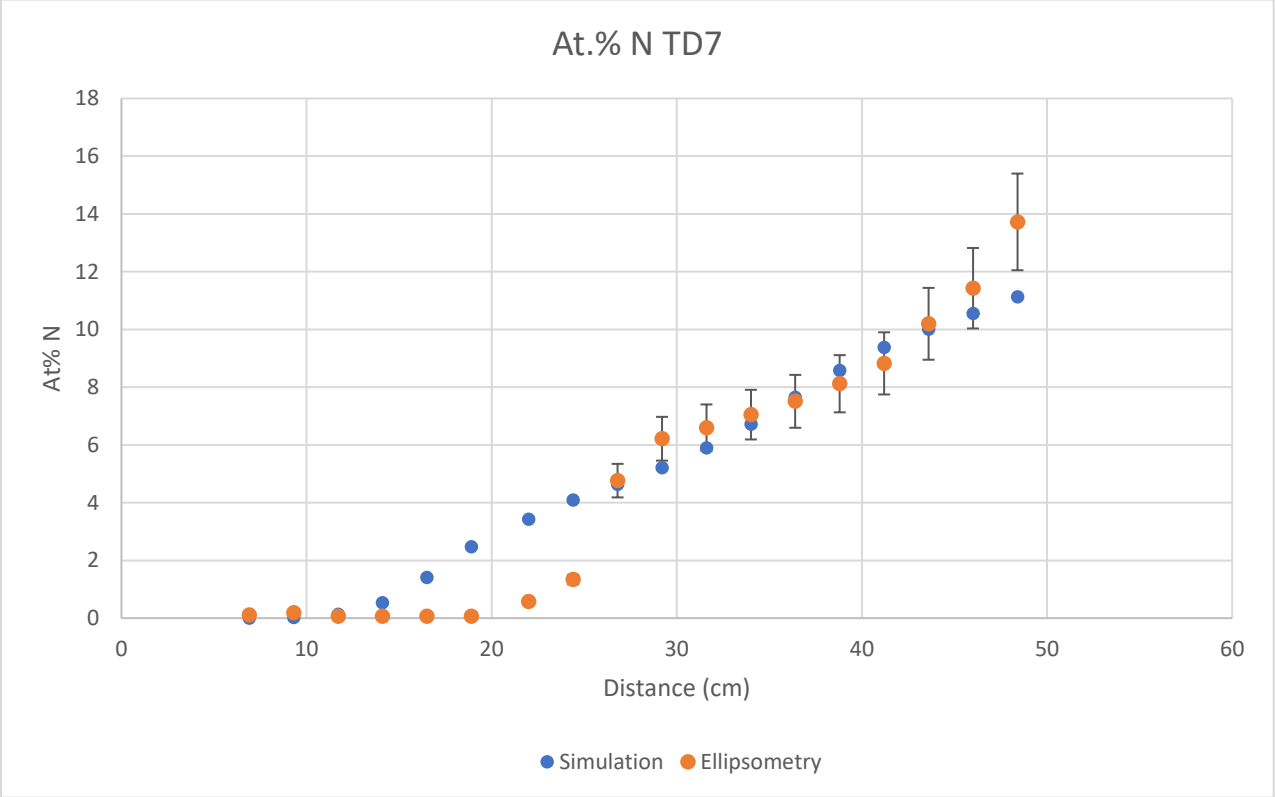

Figure 32. Comparison of the at.% of nitrogen between simulations and ellipsometry for experiment TD7.

An overestimation of the at.N% is observed at 15-25 cm of the reactor. This overestimation is a result of underestimating the SiO_2 deposition in that exact same part of the reactor.

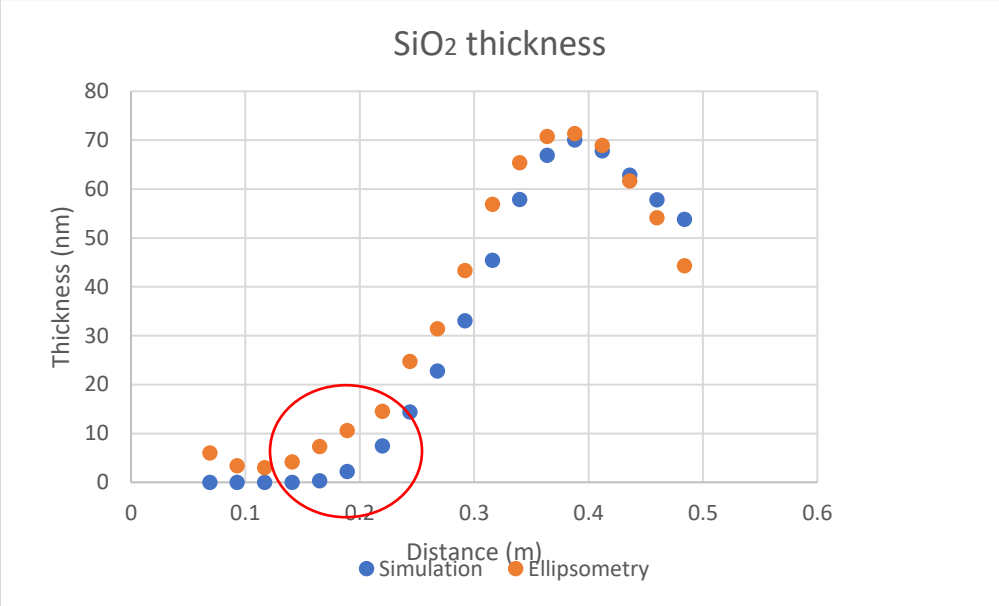

Figure 33. Divergence of the first part of the thickness profile of SiO2 between simulations and ellipsometry for experiment TD7.

There appears to be a shoulder at the start of the SiO_2 deposition which indicates that the incorporation of silica in the film happens through more than just one reaction. The issue that occurs because of that is that the position of the peak of the deposition and the starting point of the deposition cannot be fitted at the same time having just one solid phase reaction producing SiO_2 (S1). In order to have a better fit, enriching the mechanism with a new solid phase reaction producing silica would be required.

The results of the at.N% of the rest of the experiments are presented below as well as those of ellipsometry.

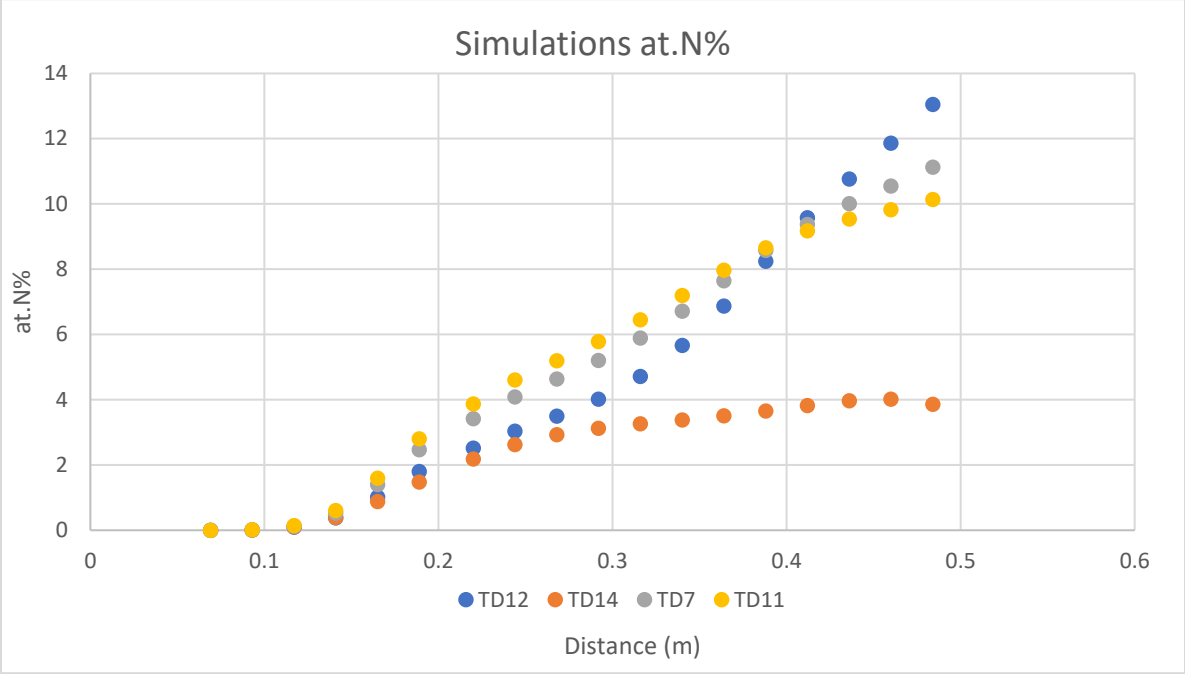

Figure 34. Comparison of the simulated at.% of nitrogen between the 4 experiments in question.

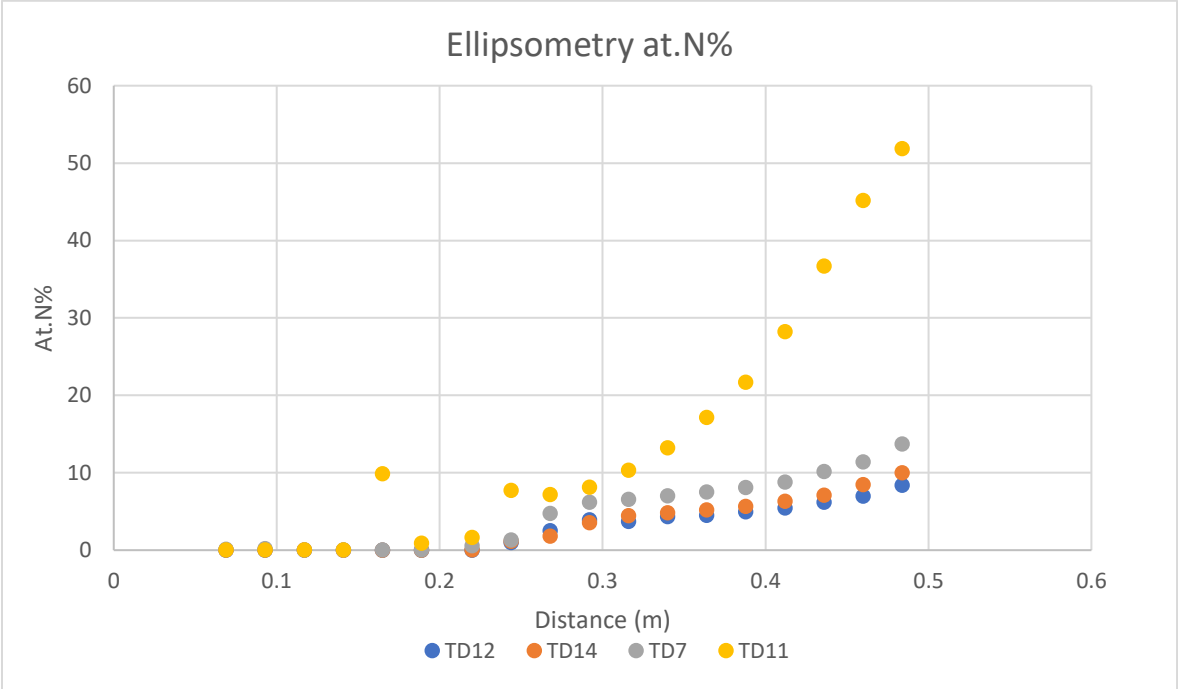

Figure 35. Comparison of the experimental at.% of nitrogen between the 4 experiments in question.

First of all, it is evident that the incorporation of N in lower temperatures is lower, since TD14 has a significantly lower at.N% throughout the whole length of the reactor. This result can be expected since the two deposition reactions (S1 and S2) are competitive to each other for the formation of the film and

since S1 is more reactive, due to the presence of O_2, we expect this difference in reactivity to be accentuated when lowering the temperature.

Furthermore, it is also proved that experiments with lower O_2 flow rate will produce film with higher at.N%. This trend can be observed in the simulations as well, where for the first 0.43m of the reactor the order of atomic nitrogen content from higher to lower between the experiments is the same as the order of lower to higher O_2 flow rate (TD11→ TD7→ TD12). After around 0.43m of the reactor though, this phenomenon seems to reverse, something that we cannot observe in the ellipsometry results and is a further indication that the kinetic model needs further refinement.

Another important observation is the significant underestimation of the nitrogen content for experiment TD11. TD11, being the experiment with the least O_2 was expected to show the highest nitrogen content, something that we can observe in both simulations and ellipsometry results. The difference in values between ellipsometry and simulations though is very significant. This observation indicates that at low concentrations of O_2, it is very probable that the kinetics change significantly, causing a much higher implementation of *N* in the film, which the current kinetic model does not account for.

Finally, we can also observe from experiment TD14, that our model cannot estimate with sufficient accuracy the atomic nitrogen percentage at different temperatures, same as with the deposition rates.

The experimental and calculated nitrogen content results of each experiment separately are presented below.

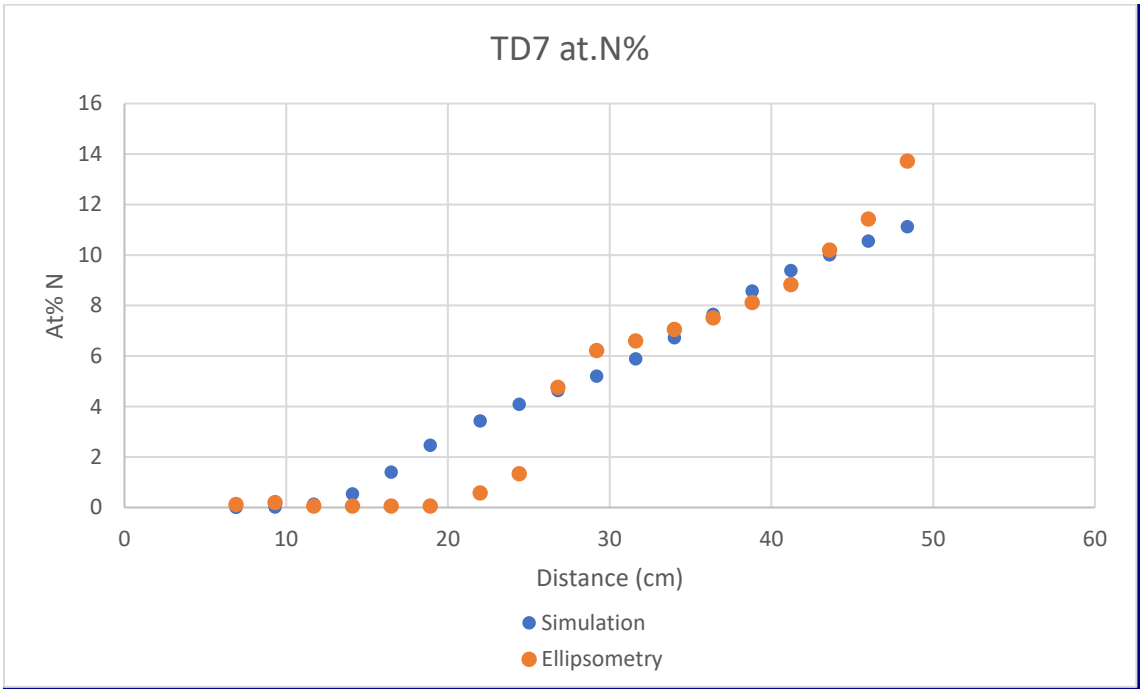

Figure 36. Comparison of the at.% of nitrogen between simulation and ellipsometry for experiment TD7.

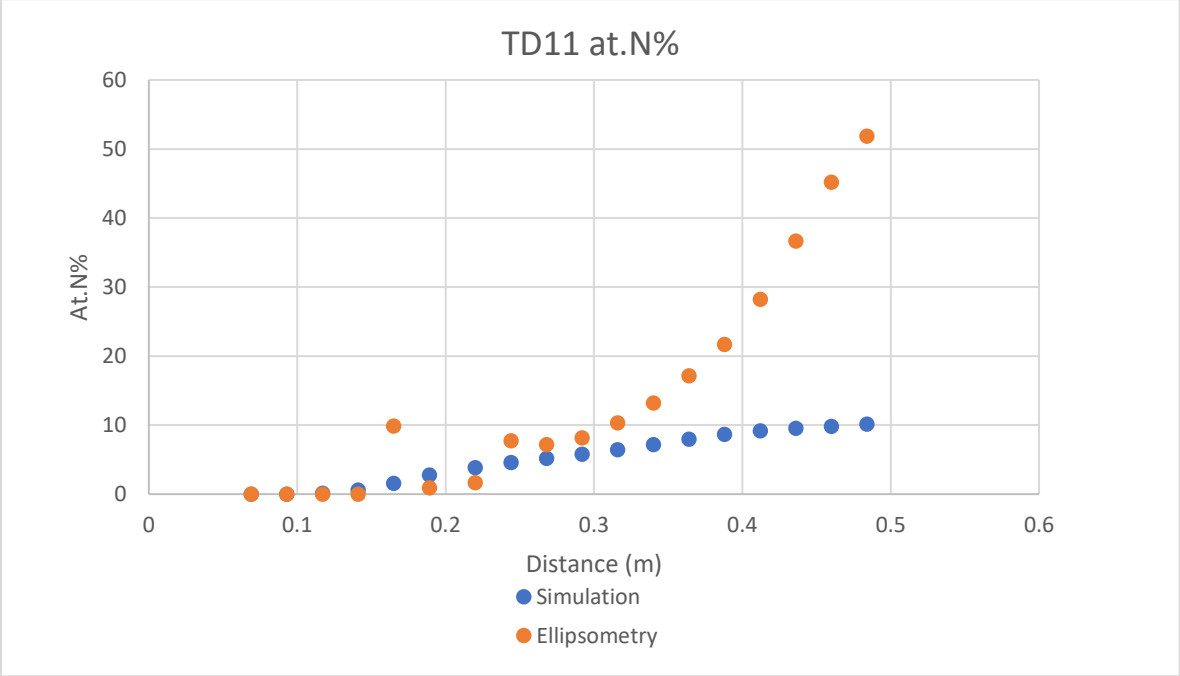

Figure 37. Comparison of the at.% of nitrogen between simulation and ellipsometry for experiment TD11.

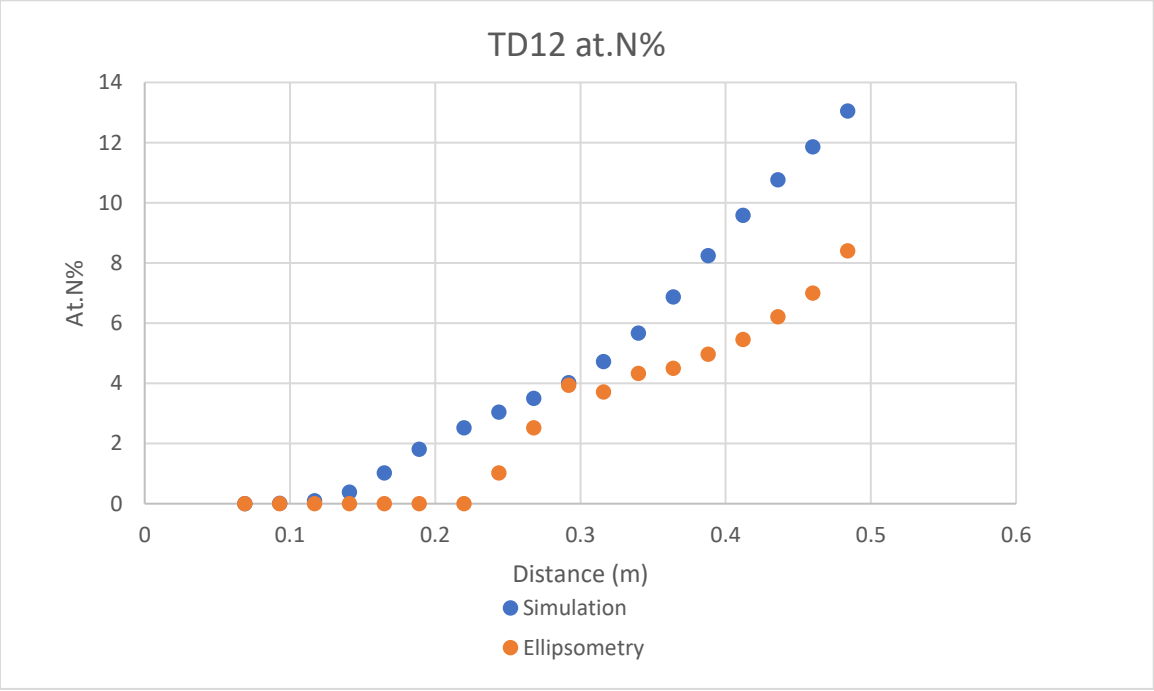

Figure 38. Comparison of the at.% of nitrogen between simulation and ellipsometry for experiment TD12.

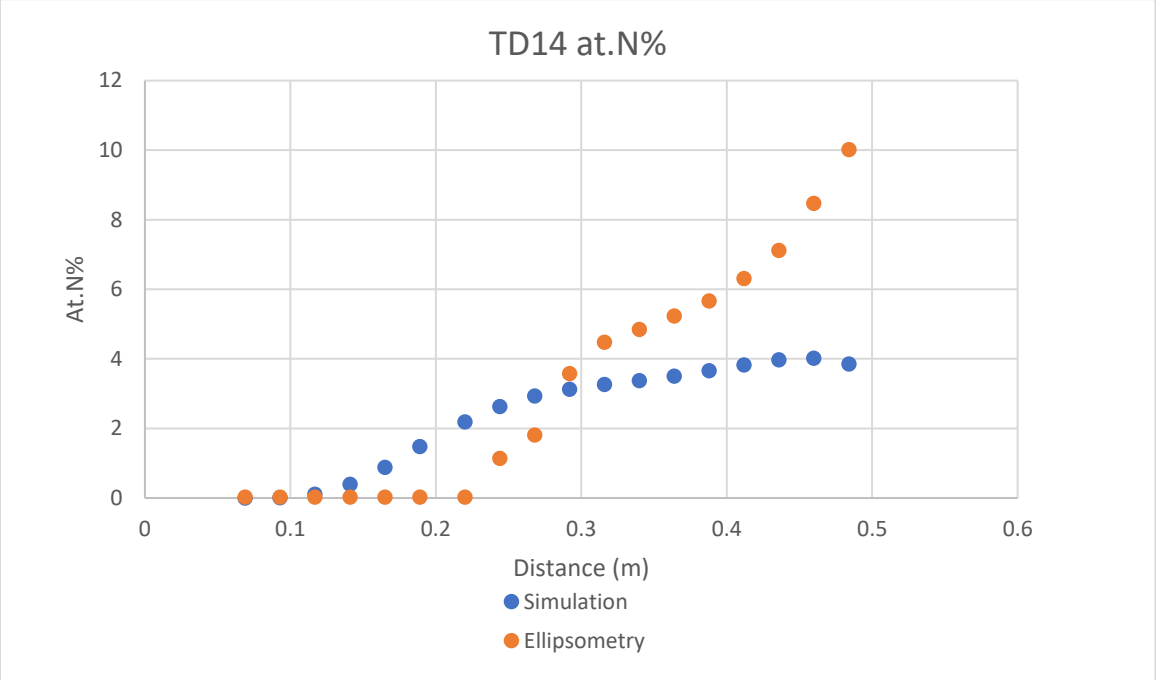

Figure 39. Comparison of the at.% of nitrogen between simulation and ellipsometry for experiment TD14.

4.5 Perspectives

Until the present point, the work done cannot be considered completely finished, mostly due to the choice of developing a very simply model. Additionally, the choice to ignore carbon, an element that has a significant contribution in the formation of the film, can also lead to errors in the simulated results. For this reason, the next part of this report will focus in methods and ways to enrich the system, in order to optimize the kinetic model further.

4.5.1 Current system optimization

The results presented, knowing the few amounts of experimental data available, must be further optimized. The imperfect fit is most evident in results replicating the atomic nitrogen percentage, where across all simulations, the nitrogen content is overestimate at the inlet part of the reactor, while the general simulated curve of the Si_3N_4 deposition appears to have a peak contrary to the curve formed by ellipsometry.

To optimize these aspects an important assumption needs to be made. The conversion of TDMSA is relatively high (81%) and at the same time the calculations for the experimental yield of TDMSA give a yield lower than 1%. As already said, it is known by the gas phase analysis that there is a plethora of by-products exiting the reactor. It is evident that the biggest amount of TDMSA is transformed into by

products and exits the reactor without participating in any film-forming reactions. In the kinetic system created, there is a very high number of intermediates (INT(Si), INT(N)) that needs to be consumed and form gas phase by-products in order to closer represent the reality of the gas phase. This way, more control over the film formation will be obtained, while at the same time as these new byproducts can be used as potential intermediates for addition reactions that lead to formation of the respective oxide and nitride film components. It has been shown that the SiO_2 deposition has a shoulder that indicates its formation from more than one reaction and thus a species, that is observed among the by-products, could be potentially used as a means to incorporate more SiO_2 forming solid phase reactions.

At the start of this project, there were unfortunately no results on the conversion of TDMSA. Waiting for these results, the simulations were being made for 50% TDMSA conversion. Compared to the 81% conversion that is followed at the moment, there was a much lower concentration of intermediates in the reactor before. Some results of these series of simulations will be presented.

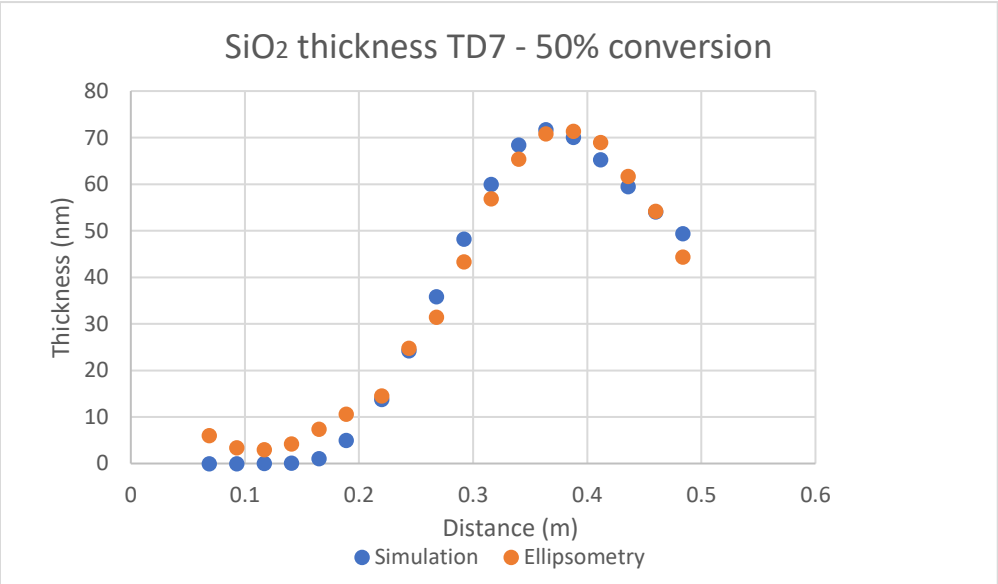

Figure 40. Comparison of the SiO_2 thickness between simulations and ellipsometry for experiment TD7 of the 50% TDMSA conversion simulation series.

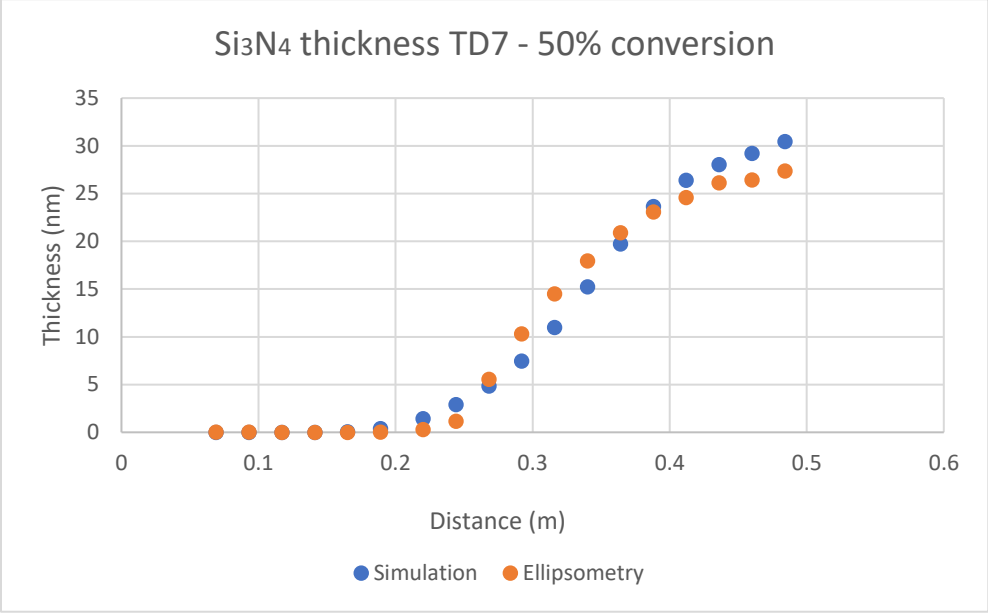

Figure 41. Comparison of the Si_3N_4 thickness between simulations and ellipsometry for experiment TD7 of the 50% TDMSA conversion simulation series.

Two things can be observed. Firstly, that the SiO_2 is a bit better fitted when fitted for 50% conversion, still there is the underestimation of the silica deposition on the first part of the reactor. Most importantly, there is no peak in the Si_3N_4 deposition when fitted for 50% conversion.

A consumption of the intermediates for the formation of by-products is thus important since it is coherent with the gas phase analysis where we observe many species exiting the reactor as well as it helps us control the deposition reactions better.

4.5.2 Carbon incorporation

The kinetic system that has been developed and implemented into the simulations is far from perfect, and thus an ongoing work. There are several points in this work that need optimization in order to end up with a concrete simulation system representing the experimental results with good accuracy, and one which can be valorized for optimizing the process.

To begin with, as explained previously, the fact that the kinetic system developed does not take carbon into account, an element, which is known to exist in the produced films and has an important influence on its structure. The issue encountered that caused ignoring the carbon content came up as an inability of ellipsometry to create a model containing carbon. For this reason, the two-phase model was followed (SiO_2/Si_3N_4) thus giving significant error in the volumetric fractions used.

The search for a solid phase analysis that can give results on the carbon content is important to finish this work. The IBA analysis would be the most useful since it can provide the atomic composition of the films. This way, working on the atomic level assumptions of describing the film as a multiphase model would be avoided. The problem with IBA is that it is an expensive and time-consuming method making it almost impossible to have the plethora of results that ellipsometry can provide. At the same time, a strategy

could be constructed to analyze few and specifically selected samples from key points in the reactor, enough to create the kinetic model.

The final days of this thesis, a new ellipsometry model was created, based on the IBA results that were supplied to the project. This new ellipsometry model was able to account for carbon with relative accuracy on its atomic percentage, as well as that of nitrogen. However, this work, though promising in helping with the creation of a more representative kinetic system needs, further investigation and validation.

If solid-phase results containing carbon were to be considered, the chemical system would have to be enriched with reactions that introduce the carbon in the film. A way that these reactions could be introduced in the existing system could be through careful inspection of the C/N atomic ration in the films. After assuming a starting view on how carbon is incorporated in the film in relation to nitrogen and oxygen, specific amounts of CH_3 moieties would be added in each of the two intermediates.

A first proposal on how a potential kinetic system could be formulated, to incorporate the inclusion of carbon, is described below.

$$V1: TDMSA \rightarrow INT(Si) + INT(N)$$
$$V2: 3INT(Si) + 2O_2 \rightarrow siloxane + H_2O$$
$$V3: INT(N) + O_2 \rightarrow INT(N)\_lessC + \ by - products$$

$$S1: INT(Si) + O_3 \rightarrow carbonated\_SiO_2$$
$$S2: INT(N) \rightarrow carbonated\_Si_3N_4$$
$$S3: INT(N)\_lessC \rightarrow less\_carbonated\_Si_3N_4$$

The idea behind the above proposals is to introduce the carbon in the system through intermediate molecules, that already contain carbon and at the same time introduce reactions that cleavage some CH_3 ligands of the intermediates in order to regulate and control the incorporation of carbon in the film.

4.6 Conclusions

This current thesis has managed to establish a good foundation and methodology on the development of the kinetic model of the TDMSA/O_2 chemical system. Based on the use of experimental data combining both gas-phase and solid-phase results, their careful analysis and interpretation has achieved the extraction of kinetic constants for the proposed reactions. The developed chemical model has successfully managed to fit and reproduce the experimental results in the simulation software with satisfactory accuracy, despite its simplicity. Nevertheless, this work, as previously mentioned, includes several assumptions that jeopardize its validity when simulating experiments performed at different conditions. The primary conclusion is that the assumption of a mere SiO_2/Si_3N_4 two-phase system, that completely disregards the presence of carbon, leads to an inability to accurately represent certain sets of experimental conditions when simulated.

The chemistry that has been selected for this project has both positive and negative aspects. A disadvantage is that it appears to be a very complicated chemical system, based on the complexity of the TDMSA precursor. Additionally, the high energy required for the precursors decomposition translates to a very low yield, while a very significant number of gas-phase by-products, both in species and in quantity, that do not contribute to film formation, is produced at the same time. This renders the construction of the kinetic model a complicated task, having to resolve into summarizing many of the reactions into fewer, apparent ones. Because of this, many of the reactions, whose involvement in the system is significant, are overlooked, since our focus is to replicate the solid phase reactions, which constitute in fact a very small part of this specific chemical system. As such, ignoring the multitude of reactions that are possibly taking place in the gas phase, contributes to significant errors in the simulation of the gas-phase concentrations of the various species, and impacts as a result, the reaction rates of the surface reactions in which these species participate.

At the same time, the existence of carbon in the system is cause for a reformulation of the model, when taking into account that the actual material that is being formed in the reactor is a $SiO_xN_yC_zH_a$ material, rather than a much simpler SiO_xN_y one, for which the thesis was based on and worked with. In order to include the carbon in the kinetic model, careful consideration of all available gas-phase and solid-phase results is required, because its incorporation translates to an additional parameter that has to be fitted in an already very saturated system.

However, one of the advantages of this system is the novelty of the utilized chemistry, which has not been explored yet in the literature, in relation to an atmospheric thermal CVD process. Moreover, this novelty also relates to the formation of silicon oxynitrides at low temperatures, without the requirement for ammonia. While there are many aspects of the kinetic model that can be refined, the chemistry itself shows a lot of potential, solidifying the interest to further study and improve its simulation, with the aim to optimize the deposition process. For this reason, even though this work consists only of a brick, it is hoped to help future researchers construct a wall.

References

[1] LGC Toulouse (2018b). Présentation. https://lgc.cnrs.fr/presentation/. Last checked on Aug 02, 2018.

[2] LGC Toulouse (2018a). Ingénierie des réacteurs polyphasiques innovants- IRPI. https://lgc.cnrs.fr/recherche/irpi/. Last checked on Aug 02, 2018.

[3] CIRIMAT Toulouse (2018a). Présentation. http://www.cirimat.cnrs.fr/spip.php?article149. Last checked on Aug 02, 2018.

[4] CIRIMAT Toulouse (2018b). Thèmes de recherche SURF. http://www.cirimat.cnrs.fr/spip.php?article353. Last checked on Aug 02, 2018.

[5] Computational study and development of a kinetic model for the moderate temperature, atmospheric pressure chemical vapor deposition of SiO2 films from the TEOS/O3/O2 chemical system. George A. Chliavoras, LGC Master internship report July 2019

[6] Deposition of silicon nitride films using chemical vapor deposition for photovoltaic applications. K. Jhansirani, R.S.Dubey, M.A.More, Shyam Singh, November 2016.

[7] A Review: Preparation, Performance, and Applications of Silicon Oxynitride Film. Yue Shi, Liang He, Fangcao Guang, Luhai Li, Zhiqing Xin and Ruping Liu, August 2019

[8] Development of a kinetic model for the moderate temperature chemical vapor deposition of SiO2 films from tetraethyl orthosilicate and oxygen Simon Ponton, Hugues Vergnes, Diane Samélor, Daniel Sadowski, Constantin Vahlas, Brigitte Caussat, 18 July 2018.

Appendix

The UDFs of the temperature profile implementation are presented below

T=650°C thermal profile :

```
# include "udf.h"

DEFINE_PROFILE(T650,thread,nv)
{
  face_t f;
   real xc[ND_ND];
    begin_f_loop (f,thread)
    {
    F_CENTROID(xc,f,thread);
              {
if((xc[2]<0.20914))
     F_PROFILE(f,thread,nv)= -88165.022547*((xc[2])*(xc[2])*(xc[2]))
                +29102.493055*((xc[2])*(xc[2]))
                - 297.954810355*((xc[2]))
                + 464.8816784;
                          else if ((xc[2]<0.6))
                F_PROFILE(f,thread,nv)=-1893241.976*((xc[2])*(xc[2])*(xc[2])*(xc[2])*(xc[2])*(xc[2]))
                + 4278394.077*((xc[2])*(xc[2])*(xc[2])*(xc[2])*(xc[2]))
                - 3952366.297*((xc[2])*(xc[2])*(xc[2])*(xc[2]))
                + 1909959.967*((xc[2])*(xc[2])*(xc[2]))
                - 510319.7429*((xc[2])*(xc[2]))
                + 71992.35814*((xc[2]))
                - 3330.025407;
                else
                F_PROFILE(f,thread,nv)= 831.789;
                                        }
                end_f_loop(f,thread)
```

```
}
}
```

T=625°C thermal profile :

```
# include "udf.h"

DEFINE_PROFILE(T625,thread,nv)
{
  face_t f;
   real xc[ND_ND];
    begin_f_loop (f,thread)
    {
    F_CENTROID(xc,f,thread);
                {
if((xc[2]<0.134))
     F_PROFILE(f,thread,nv)= -113205.59*((xc[2])*(xc[2])*(xc[2]))
                 +39807.72*((xc[2])*(xc[2]))
                - 1118.73*((xc[2]))
                 + 438.44;
                          else if ((xc[2]<0.6))
                F_PROFILE(f,thread,nv)=         - 52069.414*((xc[2])*(xc[2])*(xc[2])*(xc[2]))
                + 75454.43*((xc[2])*(xc[2])*(xc[2]))
                - 40911.265*((xc[2])*(xc[2]))
                + 9952.5*((xc[2]))
                - 32.86;
                else
                F_PROFILE(f,thread,nv)= 760.548;
                                        }
                end_f_loop(f,thread)
}
}
```